Underwater Object Localization Using a Biomimetic Binaural Sonar

by

Qiang Wang

B.Sc., Electrical Engineering
University of Science and Technology of China, P. R. China (1991)

Submitted to the Department of Ocean Engineering
in partial fulfillment of the requirements for the degree of

Master of Science in Oceanographic Engineering

at the

MASSACHUSETTS INSTITUTE OF TECHNOLOGY

and the

WOODS HOLE OCEANOGRAPHIC INSTITUTION

May 1999

Author .....
Department of Ocean Engineering
May 7, 1999

Certified by .....
John J. Leonard
Assistant Professor of Ocean Engineering
Thesis Supervisor

Accepted by .....
Professor Michael Triantafyllou
Chairman, Joint Committee for Applied Ocean Science and Engineering,
MIT/WHOI

Underwater Object Localization Using a Biomimetic Binaural Sonar

by

Qiang Wang

Submitted to the Department of Ocean Engineering
on May 7, 1999, in partial fulfillment of the
requirements for the degree of
Master of Science in Oceanographic Engineering

Abstract

This thesis describes an active wide-beam wide-band sonar system that mimics the binaural configuration of an echolocation dolphin. The system is being developed for testing new methods for underwater vehicle navigation and mapping. The system uses three 500 KHz transducers, one as transmitter/receiver and the other two as receivers. Simulations and experiments are performed in which a static point obstacle in a two-dimensional environment is detected and localized using this system. The range and azimuth of the object are determined based on the time-of-flight measurements of binaural echoes. Two basic signal detection and estimation methods for echolocation are evaluated. Amplitude threshold detection is simple but not robust and accurate enough in situations with a low signal to noise ratio. Matched filter detection is more accurate but also more computationally expensive. An improved matched method that performs matched filtering locally is suggested. A method for using the system to estimate the curvature of objects is also presented. Suggestions are made for future research that uses the system to perform dynamic sonar mapping and navigation experiments, in which the motion and scanning angle of the sonar are adaptively controlled to classify and localize objects efficiently.

Thesis Supervisor: John J. Leonard
Title: Assistant Professor of Ocean Engineering

Acknowledgments

I would like to express my deepest gratitude to my thesis advisor Professor John J. Leonard for his continuous motivation, guidance and support throughout my study and life.

Special thanks to Hans Jacob Feder for his invaluable help and encouragement during my study in M.I.T.

Thanks also to:

Wen Xu: for many happy discussions in both academic and life.

Yanwu Zhang: for being a very nice friend.

Guangyu Wu and Xiaohui Zhou: for playing Ping-Pong with me and much help on computer knowledge.

Everyone with the Design Lab:

Fred Baker: for a lot of help in preparing my presentation slides.

Kristin Gunst: for teaching me English.

Guoxing Yu, Guoling Shen and Hongye Liu: for friendship.

Everyone with the Marine Robotics Lab:

Joon, Rick, Tang, Chris and Tom, for a friendly and helpful environment.

Last, my sincere appreciation to my family: my parents, my wife and my brothers for their continuing love and understanding with affection while I was complete this degree.

This thesis is supported by Draper Laboratories under University IRD Project 98-1002 and NSF under grant 9733040.

Contents

List of Figures

Chapter 1

Introduction

1.1 Sonar data interpretation

The mobile robots used in industry today have very limited perception capabilities. They can only perform very specific tasks in well-structured environments. In the future, it is envisioned that mobile robots can be useful for many different types of applications. Examples of such application environments include factories, household, office and hospital chores, transportation, security guarding, fire-fighting, assembling structures in outer space,radioactive and other tasks dangerous for humans to perform [15]. The realization of these systems will require that we solve many challenging issues in sensor data interpretation. While the operation of mobile robot systems presents great challenges in all types of environments, the issues faced are particularly difficult for underwater robots.

Among all of these applications, extracting the information from the sensing data correctly and efficiently is a key task, which is not easy to accomplish. The major problem is how to deal with the uncertainty in the environment and how to understand the data. The development of sensors for robot applications has been under research for over twenty years, but robust and reliable interpretation of sensor data remains a difficult issue for complex, unstructured and unknown environments.

The major sensor systems which has been used in robotics research include CCD cameras, infrared ranging sensors, and acoustic transducer systems. Our motivation of

using sonar system comes from the excellent performance of natural sonar sensing, as exhibited by bats and dolphins. For land robots, acoustic sensors provide a convenient and inexpensive means for determining the proximity of objects. Particularly in the turbid and dark underwater environment, acoustic sensing becomes indispensable. Many examples have demonstrated the successful use of such sensors for mobile robot navigation, path planning, obstacle avoidance and sonar map building. However, many difficult issues remain for future research.

The main problem with sonar systems is that the observed measurements require interpretation to obtain reliable results [24]. Sensors become intelligent when appropriate signal processing algorithms are used to interpret the collection data. One consideration of interpretation is based on the physical principles of the sensor model, sound propagation, reflections and the environment.

The slow speed of the sound waves makes it easy to use a sonar system to find the travel distance of sound waves by time-of-flight (TOF) measurements. Hence, TOF estimation has become a popular and simple way to extract range information from sonar data. Different approaches have existed for TOF estimation. Among them, the most simple one is the threshold method. By detecting the time at which the amplitude of the received echo first exceeds the preset threshold level, the TOF value is also determined. The travel distance associated with the TOF reading is obtained by Equation (1.1):

$$D = C * TOF, \tag{1.1}$$

where, C is the speed of sound.

Two main problems in the interpretation of the TOF values are:

1. Objects can not always been detected even if they are within the range of the beam pattern due to noise and specular reflections.

2. The range estimate associated with the TOF value does not always correspond to the line-to-sight range of objects [24].

Because the TOF value is determined by detecting the echo amplitude and finding the first return that exceeds the threshold level, later echoes are ignored. This can be an

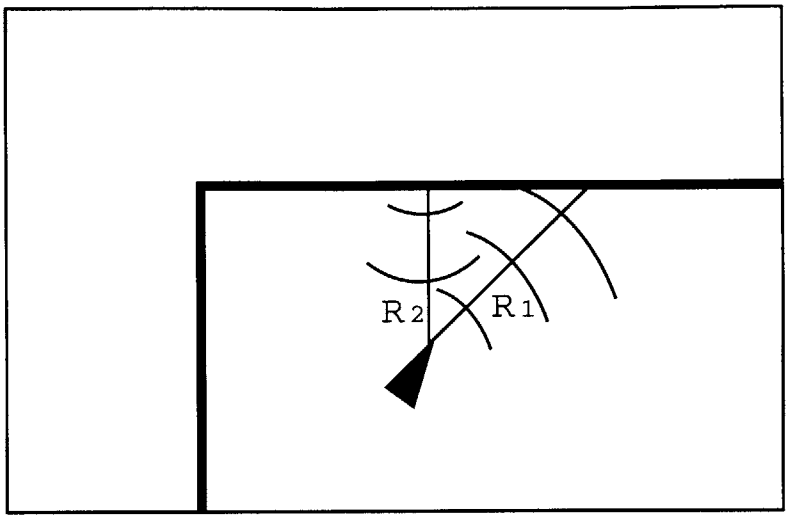

Figure 1-1: Single transducer sonar sensing system and plane reflector. In the figure, the small triangle represents a robot equipped with a sonar sensing system. It projects sound wave along the direction shown. R_1 is the range value that one might expect to receive if the transducer is pointed in the direction of robot. Yet the TOF estimation of the range is R_2, because the detected echo comes from the perpendicular reflection from the wall.

advantage, because multiple reflections from the same object are not necessary to be considered. The multi-reflections from other obstacles that might lead to estimation error can also be avoided. This is similar to an isolation effect caused by the first echo. This is illustrated in Figure 1-1.

Sonar has often been considered a poor sensor due to the difficulty of interpretation caused by poor directionality of beam pattern, noise and multiple reflections [26]. Due to these these problems, many researchers tend to abandon sonar systems or added additional sensing tools as we mentioned above, such as infrared sensors, laser ranging systems or structured light and vision systems. Yet these systems have their severe limitations for underwater robots and may be more expensive computationally and time-consuming to operate. Inspired by the strength of natural sonar systems such as bats and dolphins, our approach is to employ principles from biosonar to extend the utility of sonar systems for underwater robot systems.

1.2 The biosonar capability of dolphins

Nature is always the mother of science. Many great innovations come from careful observations of nature. It was Mcbridge who first noticed that dolphins might use echolocation for orientation, navigation, or food finding in 1958 [1]. Kellogg and his group provided the first experimental demonstration of echolocation in bottlenosed dolphins [21]. Subsequently, many scientists and researchers have investigated extensively the biosonar capability of many different species of cetaceans [35]. In this section, we will list just a few of the capabilities that have been documented. Au's book provides the definitive summary of dolphin echolocation [1].

Busnel and Dziedzic [13] provided demonstrations that a harbor porpoise could swim between 0.5 mm diameter wires without contacting them 90% of the time. Large-sized objects were rarely touched. This is an impressive capability; it would be highly desirable to provide underwater vehicles with similar capabilities.

The ability of dolphins to resolve size differences by echolocation had also been studied by many researchers. For example, Turner and Norris found that a bottlenosed dolphin, if trained in advance, could discriminate between steel ball bearings 6.35 cm and 5.08 cm in diameter, a diameter ratio of 1.25.

A basic standard in evaluating a sonar system is to determine the maximum distance at which it can reliably detect an object. An experiment done by Murchison and Penner showed that a bottlenosed dolphin could detect a water-filled 7.62 cm diameter steel sphere, with a reflective strength of -23.8 dB, at about 70 meters range. Au reports similar results [1].

Dolphins, beluga whales and false killer whales can perceive small targets as far as 110 m far away. The can classify target shapes independent of internal target reverberation. They can discriminate wall thickness differences in targets of less than 2 mm. They can operate in high noise environments [29] and [4]. And, they can detect targets buried in sediments [33].

Dolphins are also very capable at detecting signals in noise. The ideal receiver is referred to as a receiver that can yield the best detection performance in a white noise

environment according to detection theory. No receiver could exceed the performance of the ideal receiver, which generates the maximum signal to noise ratio (SNR). The ideal receiver is an important standard for evaluating the receiving capability of sonar. Au describes the comparison of a dolphin with an ideal receiver by detection of electronic phantom targets in noise [1]. Results showed that an optimal receiver would outperform the dolphin sonar by around 7.4 dB. However, other experiments showed that cetacea can perform better than an optimal detector [1].

Most of our understanding of biosonar behavior comes from static experiments [1]. There is still much interest concerning biosonar in natural settings. For example, is sonar used for large-scale navigation? How often is sonar utilized in the wild, and for what purposes?

It is safe to say that at this time no man-made sonar system can fully match the capabilities of the dolphin [28]. All of this evidence causes us to reflect: "can we learn from dolphin sonar systems for enhancing the sonar capabilities of underwater robots?"

1.3 Thesis road-map

In this chapter, some difficulties of sonar-based robotics were discussed. The capabilities of biosonar systems, such as dolphin sonar, that provide the motivation for our research were surveyed. The structure of the rest of the thesis is as follows:

Chapter Two provides a summary of previous similar research and some recent progress. Different sonar systems used in underwater and land robots are summarized. Notable custom sonar systems that have been created are reviewed.

Chapter Three presents the details of our biomimetic binaural sonar system. The hardware, software, and signal processing aspects of the system are explained.

Chapter Four illustrates the performance of the system. Techniques from waveform analysis are used to discuss the resolution of the system. Different signal processing methods for echo detection and TOF estimation will be compared. Simulations and experimental results for localization of objects are presented. An improved data

post-processing method is proposed. The problem of estimating the curvature of objects is investigated.

Finally, Chapter Five concludes the dissertation with a summary of our research. Possible applications of this biomimetic binaural system and suggestions for future research in this area are proposed.

Chapter 2

A Review of Previous Research

There has been a great deal of previous research in using sonar for robotics. This chapter will briefly review some of the most notable sonar systems that have been developed in the past that are related to our objectives. The pioneering work in this area has been performed by Kuc and his associates at Yale.

2.1 Underwater and land sonar systems

There are many different types of underwater sonar systems [39], including side-scan sonar systems, mechanically-scanned sonars, and electronically-scanned sonars. In typical underwater sonar systems, a very narrow beam is used, to increase the image quality. For example, Figure 2-1 shows a typical scan from a 675 kHz Imagenex sector-scan sonar with a ± 0.5 degree beam. As can be seen from the Figure, with a narrow beam, an "image" of an environment that is analogous to a visual image can be obtained. The image takes a long time to acquire (about 20 seconds for this sensor), and has limited spatial resolution.

Biosonar systems however, use wide beams. With a ± 5 degree beam, the corresponding picture for Figure 2-1 would look very bad. However, as discussed in the previous chapter, biosonar systems achieve very high resolution. How this exactly occurs is unknown. However, it seems that a different type of interpretation than visual image processing is being performed.

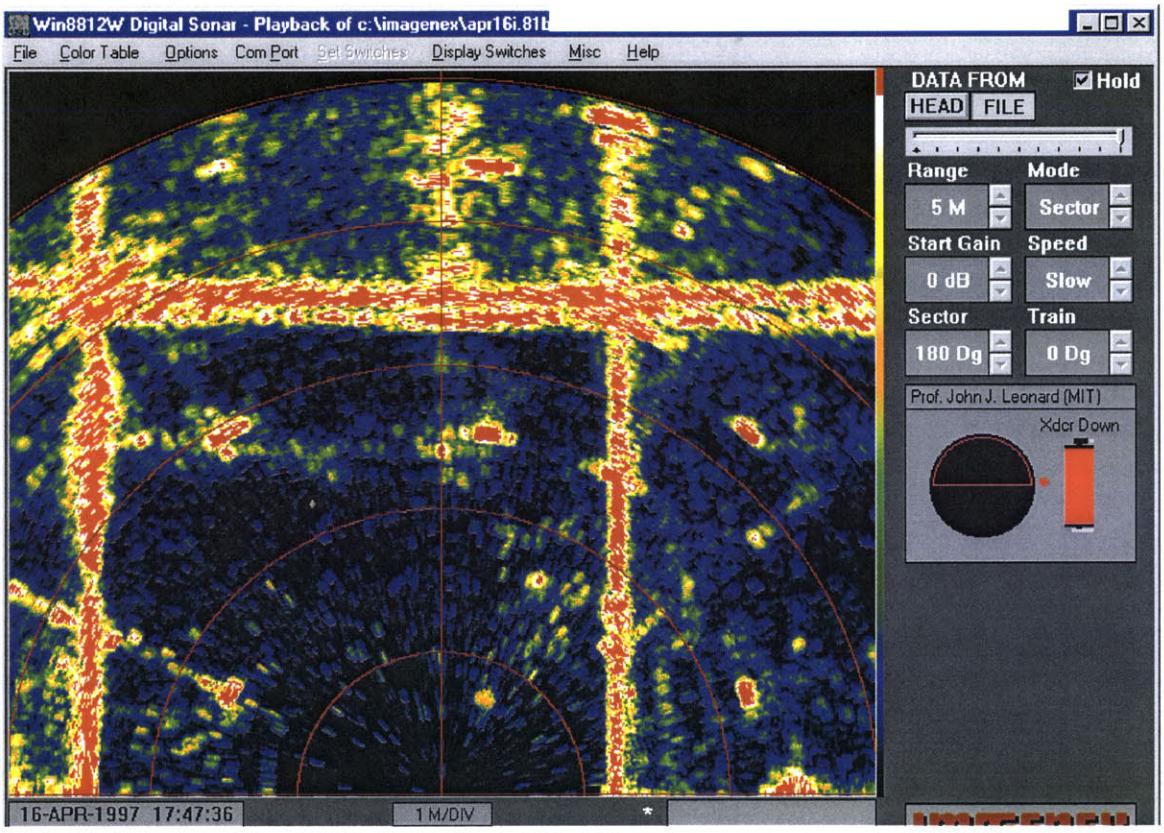

Figure 2-1: A typical scan from the Imagenex 675 kHz sector-scan sonar. The figure shows a horizontal scan of a 3 by 3 meter tank with four posts in the different quadrants of the tank.

Figure 2-2: Various acoustic transducers. The figure shows an Imagemenex 675 kHz sector-scan sonar, several omnidirectional hydrophones, a linear array for a medical imaging sonar, and several high frequency non-destructive testing transducers.

In contrast, land robot sonar systems use wide beams. This is because of the wide availability of the Polaroid ranging system hardware. There are two typical systems: (1) scanning of a single sensor, and (2) a ring of static transducers. These are shown in Figure 2-2 and Figure 2-3.

2.2 Single sensor systems

Ultrasound mechanical scanning systems are commonly used in advanced robotics applications to obtain information about the physical structure of the robotic operational environment [41]. A typical mechanical system uses electrical motors to drive a single or a few ultrasound transducers to scan interesting regions of the environment to detect potential targets.

Usually the transducer acts as both the transmitter and receiver. A modulated pulse signal is first transmitted. When it hits an object, the echo signals will be detected by the same transducer as a receiver. The spatial sensing resolution of such a conventional ultrasound transducer is limited by the beam width associated with the transducer.

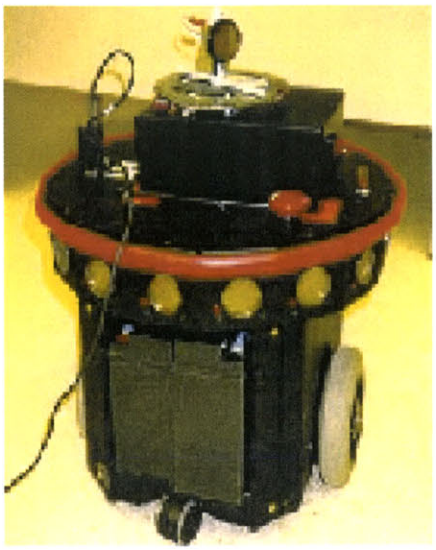

Figure 2-3: Robot equipped with a ring sonar and a scanning sonar.

For an expectation of high spatial resolution, a transducer with a narrower beamwidth is desired. However, in order to cover a specific space region we are interested, more scanning steps will be required with such a transducer. This is not good for a robot to implement a real-time task, since more scanning steps mean more acquisition and processing time [7]. Hence there is a trade-off between a wide and a narrow beam. Using a 3 dB beamwidth of about $\pm$ 5 degrees [26] seems to be a good compromise.

Leonard has used data from a single scanning sonar to demonstrate accurate feature-based sonar mapping [26]. This work, however, assumed that accurate navigation was available. Also, data acquisition to acquire detailed information was very slow. By extracting the feature of RCDs (region of constant depth) from the scannings of single sonar, Leonard proposed and implemented a unified approach for sonar-based navigation, localization, obstacle detection and map building in a multi-target environment.

2.3 Ring sensor systems

An alternative strategy is to mount the multiple transducers around the robot in a ring array. A ring of 24 sonars is the most usually employed configuration [8]. In such

a ring, 24 transducers are employed with a 15 degree angular difference between the orientation of adjacent transducers. Ring transducers improve time efficiency because they save the need of rotation with the cost of the increase of number of transducers. However in these system the robot still just processes the information coming from individual sensor instead of integrating the information coming from all transducers together. Individual echoes are only detected by the transmitting transducer.

Ring sonar sensors are primarily used for obstacle avoidance and grid-based mapping. In a grid-based method, a map of the environment is generated with an occupancy grid according to probability distribution information [37]. A grid is a representation where the measurement comes from. Each grid in the map expresses a probabilistic estimate of object occupancy. Every time when the echo signal is detected, single or multiple grids in the map are updated. This method does not require a priori information and was first proposed and investigated by Moravec [31]. Perhaps the most impressive grid-based obstacle avoidance has been performed by Borenstein [9], using the Vector Field Histogram method.

While ring sonars have been used for grid-based mapping and obstacle avoidance with success, they have not been successfully used for more detailed feature-based modeling. For this, custom sonar arrays have been developed.

2.4 Multi-element widebeam array sensor systems

Compared with the slow dynamic response due to the mechanical inertial of a single sensor system and the poor accuracy of a ring sensor system, a well known alternative approach to object localization is the use of an array of sonars. Kuroda developed a planar ultrasonic array that consisted of twenty-one transmitters, and demonstrated that an ultrasonic phased array can be a substitute for an ultrasonic mechanical scanning system [25].

Macovski studied several ultrasonic phased arrays for ultrasonic imaging used in medical and underwater applications [27]. Higuchi presented a small size electrostatic ultrasonic linear array which is composed of 32 elements. Linearly arranged on a

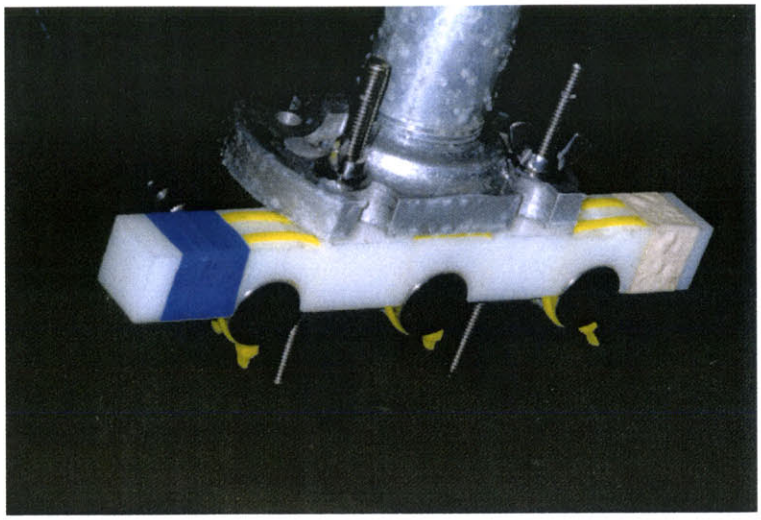

Figure 2-4: Sonar array

$20\ mm \times 30\ mm$ silicon wafer [19] using silicon IC fabrication technology, it has a high electro-acoustical transformation efficiency. Munro built a multi-receiver ultrasonic linear array, but did not propose an appropriate beam steering algorithm for source object localization [32].

The pioneer in the area of the development of intelligent multi-element sonar arrays in robotics has been Kuc. He advocates the use of a physically based sonar model to aid interpretation [24]. Barshan and Kuc developed multiple transducer arrays that can identify different object types, such as planes and corners [6]. Bozma and Kuc investigated sonar mapping for both smooth and rough surfaces and incorporated the energy and duration of sonar signals [10, 12, 11]. Kleeman and Kuc developed an optimal sonar array that could classify all three target types (corner, plane, and edge) with one scan with high accuracy [22].

Most recently, Kuc developed a system that uses waveform template matching for object recognition [23]. By mimicing the configuration of bats' sonar, Kuc built a biological echo-location system with a center transmitter flanked by two adjustable receivers. According to the echo information collected by the two receivers, the sonar system can adaptively translate or rotate its transmitter and receivers to maximize the echo intensity. At each given object pose, a corresponding echo vector is generated

associated with it. By comparing the binaural echo patterns with a data base that is constructed during a learning phase, rubber O-rings with different sizes and the head and tail sides of a coin were successfully recognized.

Peremans *et al.* [5, 34] have developed a tri-aural sonar sensor that can classify different target types and localize multiple objects with high accuracy. The system consists of three transducers lined up with a separation of d=15 cm. The center transducer acted as both a transmitter and a receiver. The two side transducers are used solely as receivers. Except that the center transmitter is also used as a receiver, the sensor arrangement of Peremans' system is the same as that used by bats. They implemented an approximate method for curvature estimation, but concluded that it was too noise sensitive to give good curvature estimates with real data. However, they used the curvature estimate for classification of objects into the categories of point objects, line objects, or unknown objects.

2.5 Summary

This chapter has reviewed previous research in using sonar in robotics. The most notable systems are those by Peremans *et al.* and by Kuc and associates, which have demonstrated impressive capabilities to classify and localize objects using air sonar. We now proceed to discuss the underwater system we have created in the next chapter.

Chapter 3

Sensing System Description

The previous chapter has reviewed previous research in sonar-based robotics and has highlighted some characteristics of biosonar that would be excellent to copy for an underwater sonar system. Based on this knowledge, this chapter describes the system that we have created. We begin by discussing the hardware for our system, then we describe the software and the signal processing system. We then proceed to describe the sonar equation parameters of the system and to discuss a sonar signal model.

3.1 Hardware description

Figure 3-1 illustrates the different components of the system. A brief overview of the operation is as follows: The pulser/receiver generates a high-voltage transmit pulse and outputs it to the central sonar transducer of the array, which serves as the transmitter. The transmitter projects the sound wave into the water. When it encounters an object in the tank, an echo will be reflected back. The reflected echoes are detected by all three receivers, two acting as the left and right receivers, and the transmit transducer acting as the center receiver. The left and right received signals are amplified by battery-powered Panametrics pre-amplifiers. The signal received by the center transducer is amplified by the pulser-receiver. All three received signals are passed to A/D data acquisition cards in a PC. The A/D boards convert the analog signals into digital data and make it available to a matlab program running on the

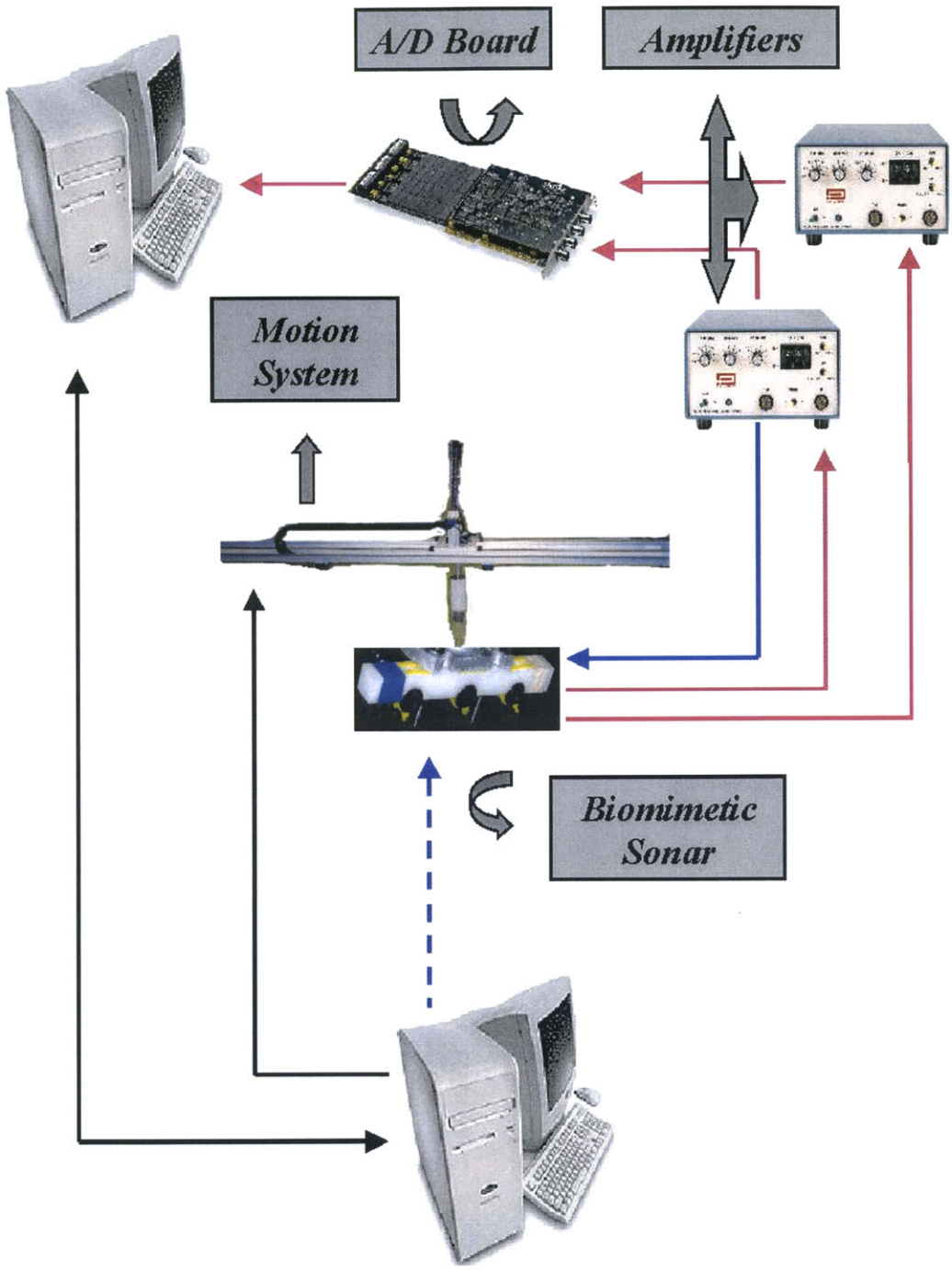

Figure 3-1: Configuration of biomimetic sonar system. The biomimetic sonar arrays are mounted on the motion system. The blue line shows the direction of outbound signal, while the red lines show the direction of the inbound signal. The A/D board is plugged into on PC. The two computers communicate by the internet.

PC. A second PC is used to control the motion system. Based on analysis of the data, the motion system will be moved to a new location for acquisition of more acoustic data. The process can be continued indefinitely, logging data to disk and processing the data to realize closed-loop sensing and motion. Each part of this system will be described in more detail below.

3.1.1 Testing tank and motion control system

Figure 3-2 illustrates the testing tank and the motion control system that was used in our research. The tank is 9 meters long by 3 meters wide by 1 meter deep. The motion system is manufactured by Parker-Hauser Corporation. It consists of a large workspace, three degree-of-freedom robot system. The system was designed to provide motion throughout the area of the tank, with two translational and one rotational degrees of freedom.

The system uses a Compumotor AT6450 multi-processor-based, four-axis servo controller which is plugged into the expansion slot of a PC. These servo controllers provide sophisticated multi-axis control with 0.1 mm accuracy. The AT6450 utilizes a dual processor approach. A microprocessor is responsible for executing high-level motion programs and a digital signal processor (DSP) implements a high-speed servo control algorithm. A separate auxiliary board simplifies connections with encoders, motor drives, joystick, limits, and programmable I/O. The system is controlled using the motion architect software package, with a program created by Feder [16].

This motion system has the following advantages that are good for underwater vehicle modeling:

1. 1 to 4 axes of optically isolated servo control, which can reduce operation noise;

2. Update rates for the servo loop as fast as 200 microseconds for one axis, which is useful for real-time control;

3. Home position limit switches and positive and negative end-of-travel limits for each axis, which can avoid the damage of the motion system.

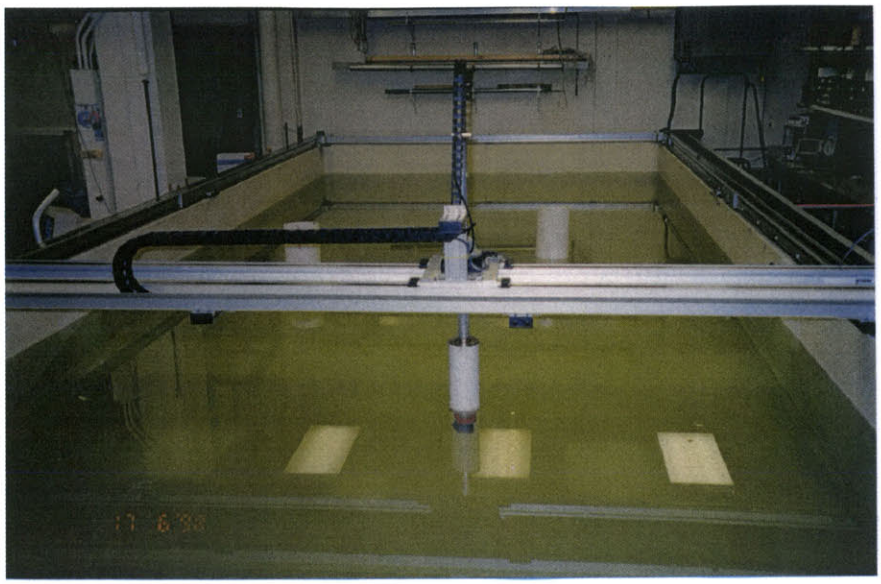

Figure 3-2: Testing tank and motion control system.

4. High position accuracy (better than 1 millimeter repeatability).

5. Joystick motion mode for easy manual operation.

3.1.2 Sonar transducers

The biomimetic sonar arrays consist of three Panametrics immersion transducers, which are specifically designed to transmit ultrasound in situations where the test part is partially or wholly immersed in fresh water. The separation between transducers is 6.5 mm.

The sonar transducers chosen for the system are the Panametrics V318 non-destructive testing transducers. These transducers are very broadband with a center frequency of about 500 kHz and a bandwidth of about 350 KHz. At this frequency, the sonar wavelength is 3 mm. The system operates at about five times the frequency of the dolphin sonar system. The 3 dB beamwidth of a circular piston transducer is given by [39]:

$$\theta_{3dB} = \pm \frac{29.5\lambda}{D} \ , \tag{3.1}$$

which for the V318 transducers gives us a value of $\pm$ 4.65 degrees. This compares

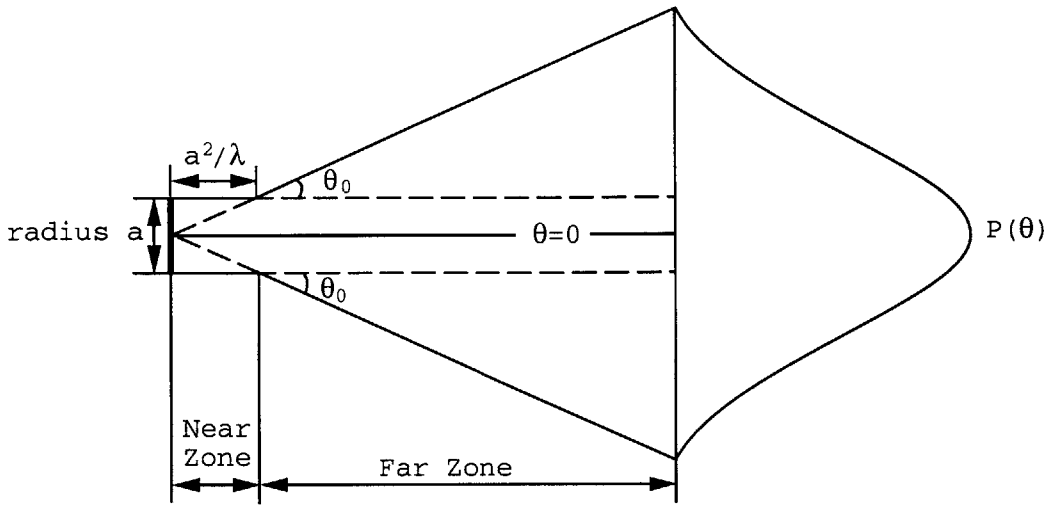

Figure 3-3: Model of sound transmission (from [6]).

very well with an average value given by Au for the bottlenose dolphin of ± 5.0 for the transmit beam pattern.

The dolphin's hearing is effectively omnidirectional. However, in our system we use 2 V318 transducers as receivers, for three reasons: convenience, availability, and simplicity. Experiments with omnidirectional hydrophones gave us poor signal levels and increased noise. Using the same transducers for receive and transmit has been very reliable. This is less "biomimetic" than with omnidirectional receivers, however, the arrangement is similar to that used in robotics by Peremans [34], Kleeman and Kuc [22], and Barshan and Kuc [6].

A physical model provided in [6] is used here to describe the sound transmission of the transducer. When the radius of the transmitting aperture, a, is much larger than the sound wavelength, λ, a directional beam is formed. We can model this kind of transmitter as a flat piston of radius a, enclosed in an infinitely large baffle, which is vibrating at a frequency f . There are two distinct regions in the produced beam pattern: the near zone (Fresnel zone) and the far zone (Fraunhofer zone).

The near zone is contained within a cylinder of diameter $2a$, where a is the radius of the transducer. The range of the near zone is approximately from the transmitter to a distance of a^2/λ.

The beam of the far zone of the transducer is limited to a beamwidth of ± 4.65

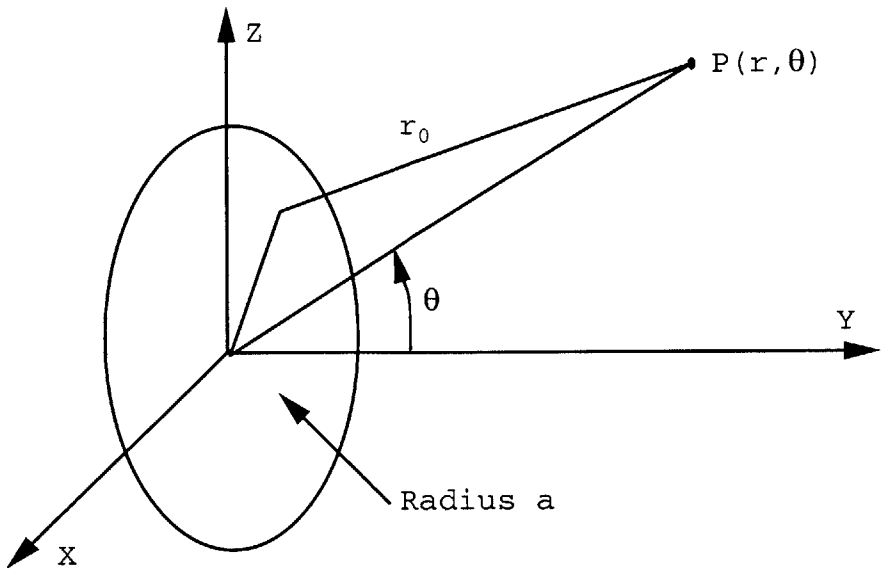

Figure 3-4: Sound pressure of a point in free sound field.

degrees. In the far zone, the projecting sound wave can be considered as plane wave.

For continuous wave transmission, the sound pressure of the transmission transducer can be modeled as:

$$P(r,\theta) = \frac{P_0}{r} \cdot \frac{J_1(Ka\sin\theta)}{Ka\sin\theta} , \tag{3.2}$$

where r is radial distance from an object point to the transducer, P_0 is the sound pressure amplitude along the line of sight to the transducer at the axis range of r_0 (as shown in Figure 3-4), θ is angle of the object point with respect to the transducer, $K = 2\pi/\lambda$ is the wave number, $\lambda = c/f$ is the wave length, and J_1 is the Bessel function of the first kind.

According to experimental results provided by Barshan and Kuc [6], equation (3.2) can be simplified to:

$$P(r,\theta) = \frac{P_0}{r} \cdot e^{-\frac{2\theta^2}{\theta_0^2}} , \tag{3.3}$$

where θ_0 is the half width angle of transducer. This is illustrated in Figure 3-4.

3.1.3 Pulser-receiver and pre-amplifiers

The transmit signal is generated by the Panametrics model 5052PR, which is a high voltage pulser-receiver. It is designed for ultrasonic test and measurement applications with a high material penetration capability. It can deliver up to 115 volts pulse excitation to proper low frequency transducers. The receiver section provides 60 dB RF gain. A full range of front panel controls permits convenient adjustments for all important instrument functions. The receiver gain is selectable from 20 to 40 dB, while the receiver attenuation is adjustable from 0 to 68 dB.

The typical features of this kind of amplifier are as following:

1. High voltage pulse, excitation up to 115 volts;
2. High gain, low noises broadband (10 MHz) receiver;
3. Pulse-echo transmission modes;
4. 40 dB RF Gain;
5. Receiver attenuation range of 0 to 68 dB;
6. Switchable high pass filters.

Model 5662 battery-powered preamplifiers provide good amplification to the left and right channels with with low-noise.

3.1.4 Data acquisition cards

The data acquisition cards used in the system are made by Gage Applied Sciences, Inc. The CompuScope 1012/PCI is a family of 20 MS/s, 12 bit IBM PC based data acquisition cards. In our system, a set of four boards are used, in two master-slave pairs. The boards are responsible for converting the analog echo signal into digital data and passing these data to the host computer for post-processing.

It has the following key features which can satisfy the speed requirements for ultrasonic signal acquisition:

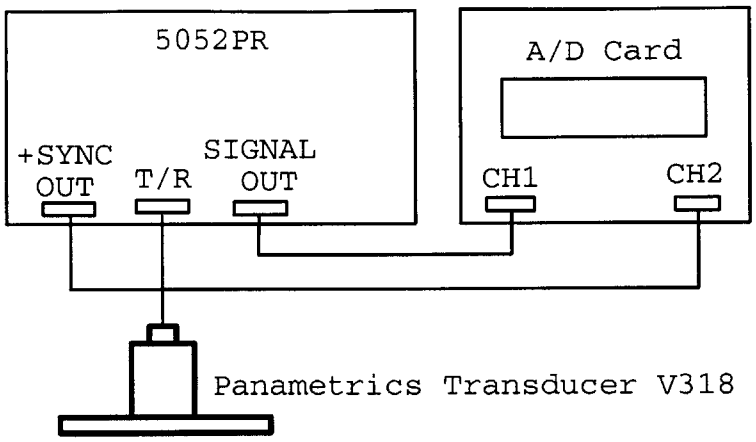

Figure 3-5: Connections between amplifier and transducer.

1. 20 MS/s, 12 Bit sampling;
2. 100 MB/s Bus throughput;
3. Flexible triggering;
4. Multiple record.

Actually, this A/D board consists of the two boards: one CS1012 analog board and one X012PCI PC interface board. All signal conditioning and A/D conversion work on the CS1012 analog board and all data storage and PCI bus interface are on the X012PCI board. This structure greatly speeds up the data transfer and reduces noise. Also, the CompuScope 1012 Data Acquisition Card provides a state-of-the-art analog triggering feature. An analog triggering level on the analog board can be easily controlled by an external signal or by software. The trigger level and slope are selectable. These functions can help select a better echo triggering level for detection according to different noise and signal conditions.

3.2 Software

The software is divided into three parts, running on two different PCs. One PC handles the motion control, and the other PC performs the sonar processing. Two

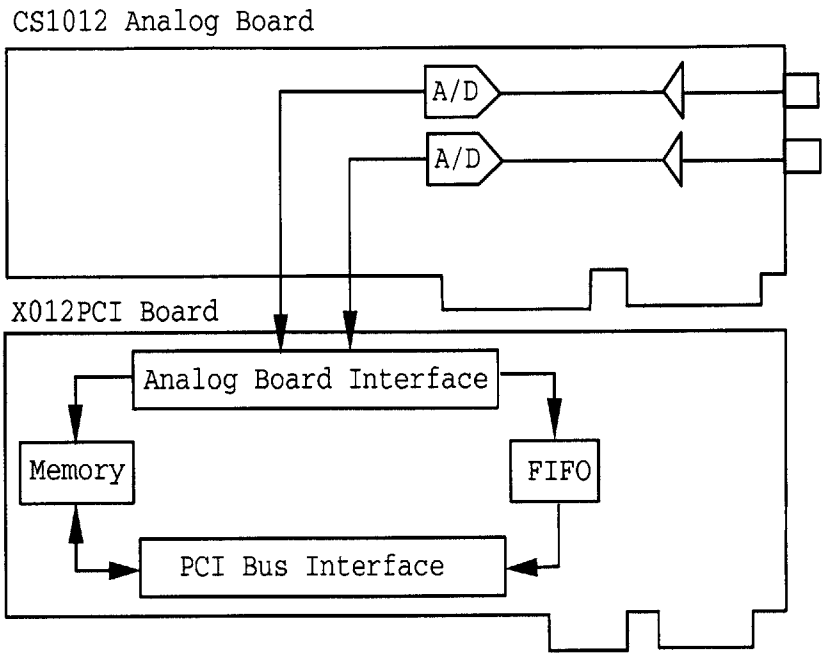

Figure 3-6: Structure of CompuScope 1012 data acquisition card (from [14]).

programs control the motion system, one running in Visual C++ and one in Matlab. The Visual C++ program is a generic interface to the motion control system, using DLL's that are part of the motion architect software control library. For ease of experimentation, the Visual C++ program is controlled indirectly using the file system on the PC by a script executing under matlab. Matlab is also used to perform the data acquisition on the sonar PC, using a DLL for the data acquisition system provided by Gage. The overall software architecture was conceived and implemented by Feder [16] and has proven very reliable and easy to use.

A block diagram for the signal processing for range and angle estimation is shown in Figure 3-7. The flow of control through the various processing steps is simply specified by a sequence of matlab commands.

Figure 3-8 shows a typical scan of the tank using data from the center channel of the sonar system [16].

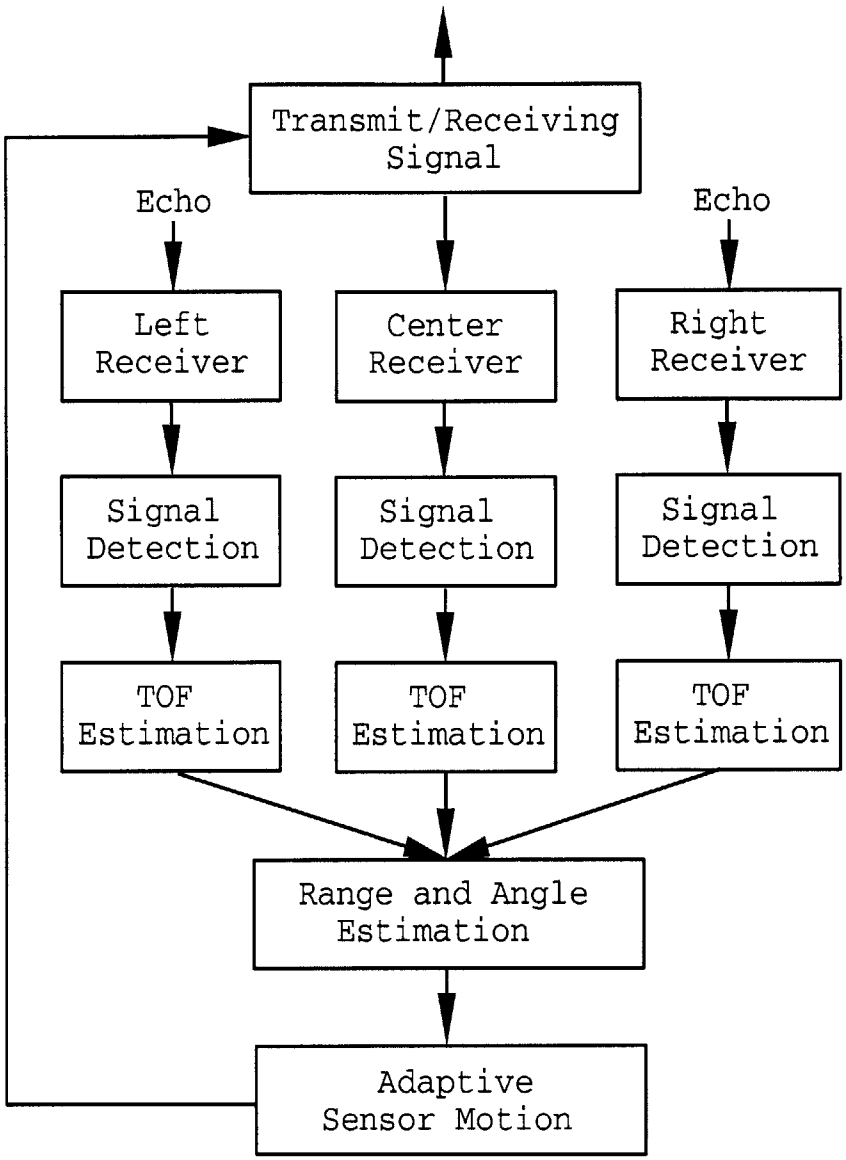

Figure 3-7: Processing diagram for the system.

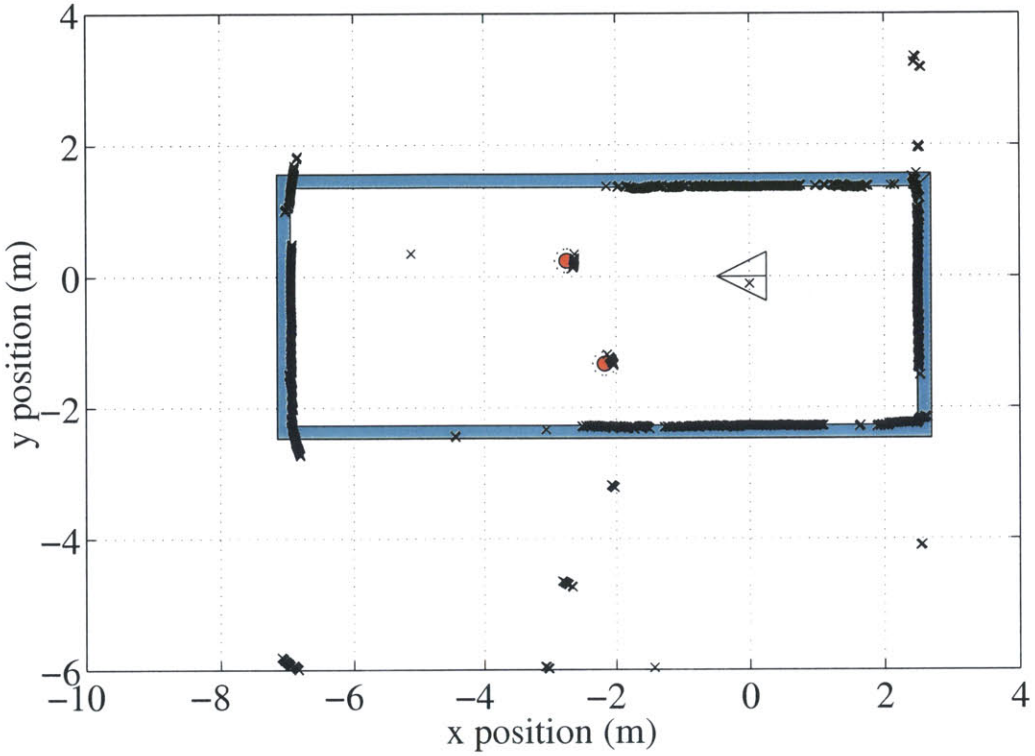

Figure 3-8: Typical scan of the system, using data from just the center transducer [16]. The blue regions designate the walls of the tank. The triangle shows the location of the sensor. The red circles show the location of 2 PVC cylinders. The black 'χ' marks designate the sonar returns.

3.3 Sonar equation analysis

For a given object, a sonar system will have a maximum range at which it is able to obtain a sufficiently strong echo to have a good detection. Sonar sensors are designed to detect echoes that exceed a certain sound energy level. The sonar equation provides a way to analyze a given situation [39]. The echo level is determined by the characteristics of the equipment, the medium, and the target. The equipment consists of the transducer, the amplifiers etc. The active sonar equation with noise background for the signal to noise ratio (SNR) of an echo is:

$$SNR = SL - 2TL + TS - NL + DI \ , \tag{3.4}$$

where, SL: projector source level;

TL : Transmission Loss;

TS : Target Strength;

NL : Noise Level;

DI : Directivity Index.

The definition of the parameters in the above equation is shown in Table 3.1.

We use the term SNR here instead of DT as in Urick [39] because we consider it more appropriate for the discussion of signal detection using different detection methods. When two different transducers are used as transmitter and receiver, the transmission loss should be separated into two terms, one the outbound loss and the other the inbound loss. However, since our transmitter and receiver are close to one another, the combination $2TL$ is used here for simplification.

For our system, it turns out that a sonar system analysis is not very useful. One reason is noise (discussed below). Another reason the sonar equation analysis is not useful is that the sonar equation analysis assumes steady-state, continuous wave sound signals. However, our system uses very short, transient signals. Urick discusses corrections to the sonar equations for transient effects, but these are difficult to apply

Table 3.1: Definition of parameters in sonar equation (from [39])

Parameter	Symbol	Reference location	Definition
Source level	SL	1 yd from source on its acoustic axis	$10\log\frac{intensity\ of\ source}{reference\ intensity}$
Transmission loss	TL	1 yd from source and at target or receiver	$10\log\frac{signal\ intensity\ at\ 1\ yd}{signal\ intensity\ at\ target}$
Target strength	TS	1 yd from acoustic center of target	$10\log\frac{echo\ intensity\ at\ 1\ yd\ from\ target}{incident\ intensity}$
Noise level	NL	At hydrophone location	$10\log\frac{noise\ intensity}{reference\ intensity}$
Receiving directivity index	DI	At hydrophone terminals	$10\log\frac{noise\ power\ by\ an\ nondirection\ hydrophone}{noise\ power\ by\ actual\ hydrophone}$

in our system. We can still calculate some of the other parameters, providing some insights. The equation to calculate the projector source level is:

$$SL = 171.5 + 10\log P + DI_T\ . \tag{3.5}$$

In our sonar system, the energy of the pulse is 94 μJ, the duration of the pulse is approximately 5 μsec. Hence the acoustic power is approximately 19 watts, so,

$$SL = 178.2 + DI_T\ . \tag{3.6}$$

For a circular piston transducer like the V318 Panametrics transducer used in our sonar system, the directivity index is calculated as:

$$DI_T = 20\log(\pi * D/\lambda) = 20\log(\pi * 0.019/0.003) = 26.0\ \text{dB}\ , \tag{3.7}$$

where 19 millimeters is is used for the diameter of the transducer. Hence, the source level SL=220 dB re 1μPa.

The principle losses of acoustic signal energy in the ocean medium are due to spherical spreading, and absorption or attenuation. We can state this as:

$$\text{Propagation loss} = \text{Spreading loss} + \text{Absorption loss} \ . \tag{3.8}$$

A simple example in usual life is that when we drop a stone in a pool, we can observe that when the wave goes further from the source, it will eventually disappear in the pool. This phenomena seems to suggest that the spherical spreading loss is essentially a function of distance or range from the source and is not a function of any other attribute of the wave such as frequency or wavelength. In a decibel expression, the loss of signal level as a function of distance or range traveled is simply expressed as:

$$\text{Spreading Loss} = 20 \log R \ , \tag{3.9}$$

where R is the range or distance from sound source. However, actually, the absorption of the underwater channel does vary with the frequency of the sound energy being transmitted. This absorption loss can be expressed as:

$$\text{Absorption Loss} = \alpha \times R \times 10^{-3} \ , \tag{3.10}$$

where α is the absorption coefficient in dB/kilometer, and R is the distance in meters. From [39], we can determine that at 500 kHz, α is approximately 100 dB/kilometer.

The target strength depends strongly on the shape and material of the object, as well as the angle at which the sonar is pointed at the object. In general, TS is only know for relatively simple shapes. For example, for a sphere:

$$\text{TS} = 10 \log \frac{r_0^2}{4} \ , \tag{3.11}$$

which means that a sphere of radius 2 meters has a 0 dB target strength. The objects we have looked at in our research are much weaker targets. Hence, they will have negative values for target strength.

There is no absolutely quiet water. The major noise sources in the ocean are thermal noise, water noise, cavitation noise, underwater animal noise, traffic noise and electric noise. In our sonar system, due to the limited propagation power of transducers and the tank environment in our laboratory, we think the electrical noise is most important. The electrical noise could be reduced in the future by mounting the power and pre-amplifiers as close as possible to the transducers. In addition, the motion system appears to create acoustical noise that effects our system, this will be more difficult to address.

In a typical oceanic sonar application, the noise is due to oceanic effects (waves etc.) and distant shipping at low frequencies. At higher frequencies (such as 500 kHz where our system operates), acoustic noise is usually accounted for by the thermal noise equation:

$$NL = -15 + 20\log f = -15 + 20\log 500 = 39 \text{ dB re } 1\ \mu\text{Pa} . \qquad (3.12)$$

However, in our system there is a great deal of electrical noise coming from the motion control system, the data acquisition PC, and other electrical equipment in the building. The electrical noise level is many orders of magnitude larger than what we would expect from purely acoustic considerations. Further, the electrical noise varies with location in the tank, with time of day, etc. Hence, at present our conclusion is that a useful sonar equation analysis for the system can not be performed.

3.4 Signal analysis

3.4.1 Signal observation model

Due to the rise and decay times of the circuits in the transducer, the filter and the receiver, there is a limitation imposed the transmitted on pulse shape. For our system, we can use Gaussian function $exp[-13.8t^2/T^2]$ as a simple approximation of the pulse envelope shown as Figure 3-9, hence the outbound signal of the sonar system can be expressed as:

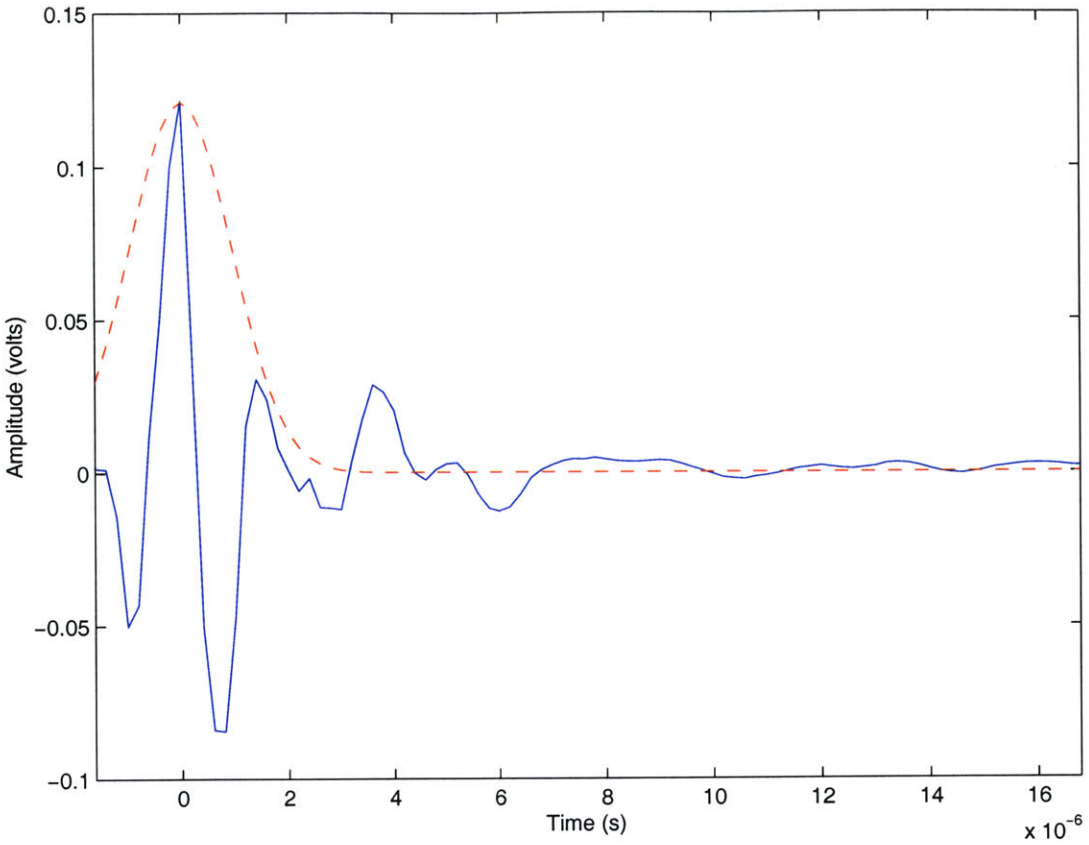

Figure 3-9: Signal observation model. The blue signal is the observed transmission signal. The red dash line shows the estimated envelope of transmission signal as a Gaussian function $exp[-13.8t^2/T^2]$

$$s(t) = k \cdot e^{-\frac{13.8t^2}{T^2}} \cdot e^{j2\pi f_0 t} \ , \tag{3.13}$$

where T is the time duration of the signal, f_0 is the central frequency of the signal, and k is an amplitude const.

3.4.2 Range and frequency resolution

The ambiguity function for a sonar system is the most important descriptor of the detection and range/Doppler estimation properties of a system. It was first introduced by Woodward and later developed in many references for evaluating the performance of the sonar system. By analyzing the ambiguity function of the transmission signal, we can know the range and frequency resolution of the sonar system. For our

simulation and experiment, the object is considered as static. The range resolution is a more important issue. We do not need considered the frequency distortion of wide-band signal caused by the motion of object.

The definition of the ambiguity function is:

$$|\chi(\tau,\varphi)|^2 = |\int_{-\infty}^{\infty} s^*(t)s(t+\tau)e^{-j2\pi\varphi t}dt|^2 = |\int_{-\infty}^{\infty} S^*(f)S(f+\varphi)e^{-j2\pi\varphi t}df|^2 \ , \quad (3.14)$$

where τ, φ is the location in the range Doppler plane, and $S(f)$ is the frequency spectrum of signal $s(t)$. If the energy of signal has been normalized, then,

$$E = \int_{-\infty}^{\infty} |s(t)|^2 dt = \int_{-\infty}^{\infty} |S(f)|^2 df = 1 \ . \quad (3.15)$$

In our system, the signal is:

$$s(t) = k \cdot e^{-\frac{t^2}{T^2}} \cdot e^{j2\pi ft} \ , \quad (3.16)$$

as described in equation (3.13).

The substitution of $s(t)$ into Equation (3.14) and the evaluation of the infinite integral with the aid of an integral table, yields:

$$|\chi(\tau,\varphi)|^2 = K_0 exp[-(\frac{13.8t^2}{T^2} + \pi^2 T^2 \varphi^2)] \ , \quad (3.17)$$

where K_0 is a const. From this equation, we can get the time (range) resolution:

$$\delta(\tau) = 0.225 \times T \ . \quad (3.18)$$

In our system, T is about $0.005ms$, so the resolution of the range is:

$$0.225 \times T \times c = 0.225 \times 0.005 \times 10^{-3} \times 1500 = 1.69 \ (mm) \ . \quad (3.19)$$

3.4.3 Range estimation accuracy analysis

When the underwater object is close to the sonar system, the process from the signal transmission to reception can be modeled as a linear process. Assuming the transmission signal is $s(t)$, then the receiving signal will be $r(t) = a \times s(t-\tau) + n(t)$. The receiving signal seems like a copy of the transmission signal with reduced amplitude and added noise (as shown in Figure 3-10).

If we move the transmission signal along the time axis with parameter τ, then the squared error between the receiving signal and the moving transmission signal is:

$$\varepsilon^2 = \int_{-\infty}^{+\infty} |s(t-\tau) - r(t)|^2 dt \ . \tag{3.20}$$

It can be extended as:

$$\varepsilon^2 = K - 2Re \int_{-\infty}^{+\infty} s(t-\tau) \cdot r(t) dt \ , \tag{3.21}$$

where, the K could be assumed as a constant and equal to the energy of transmission signal plus the energy of receiving signal. By minimizing the squared error ϵ^2, we can obtain an optimal estimate for the time delay, τ. The standard deviation of the error in estimating τ can be obtained from [1] [40]:

$$\sigma_\tau = \frac{1}{2\pi\beta\sqrt{2\frac{E}{N}}} \ , \tag{3.22}$$

where β is the bandwidth of transmission signal, E is the energy spectrum density of the transmitted signal and N is the energy spectrum density of the noise. The estimated range $R = c \times \tau$. Correspondingly, the estimation error of range should be:

$$\sigma_R = \frac{c}{2\pi\beta\sqrt{2\frac{E}{N}}} \ . \tag{3.23}$$

In our sonar system, the signal bandwidth is about 350 KHz. If we assume the

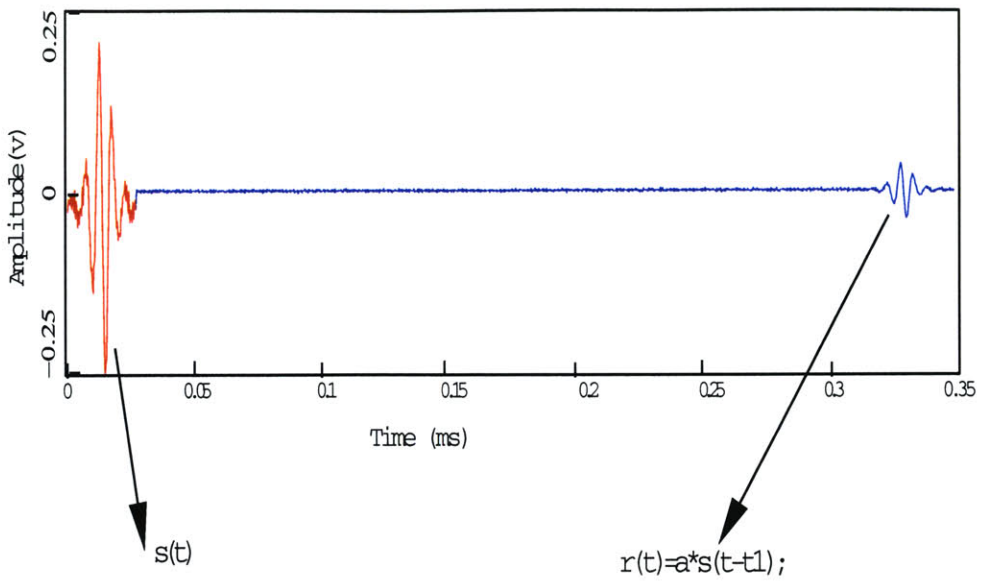

Figure 3-10: Transmitted signal and echo. The echo seems like a copy of the transmitted signal with reduced amplitude a and time delay $t1$

signal to noise ratio $SNR = E/N$ is about 5 dB, then

$$\sigma_R = \frac{1500}{2\pi \times 350 \times 10^3 \times \sqrt{10}} = 2.158 \times 10^{-4} \ (m) \ , \tag{3.24}$$

and there will be an uncertainty of 0.216 mm in range estimation.

3.4.4 Time-bandwidth product

Time-bandwidth product is another important item for evaluating the signal waveform. It seems like a kind of "uncertainty principle". The mean square bandwidth is defined as:

$$\beta^2 = \frac{\int_{-\infty}^{+\infty} (f - f_0)^2 |S(f)|^2 df}{\int_{-\infty}^{+\infty} |S(f)|^2 df} \ , \tag{3.25}$$

where the f_0 is the center frequency of the signal with definition:

$$f_0 = \frac{\int_{-\infty}^{+\infty} f |S(f)|^2 df}{\int_{-\infty}^{+\infty} |S(f)|^2 df} \ . \tag{3.26}$$

The mean square time duration of the signal can be expressed as:

$$\tau^2 = \frac{\int_{-\infty}^{+\infty} (t - t_0)^2 |s(t)|^2 dt}{\int_{-\infty}^{+\infty} |s(t)|^2 dt} , \tag{3.27}$$

where

$$t_0 = \frac{\int_{-\infty}^{+\infty} t|s(t)|^2 dt}{\int_{-\infty}^{+\infty} |s(t)|^2 dt} . \tag{3.28}$$

So, the time bandwidth product of a signal is:

$$|\tau^2 \cdot \beta^2|^{\frac{1}{2}} = \frac{\int_{-\infty}^{+\infty} t^2 |s(t)|^2 dt \cdot \int_{-\infty}^{+\infty} f^2 |S(f)|^2 df}{\int_{-\infty}^{+\infty} |s(t)|^2 dt \cdot \int_{-\infty}^{+\infty} |S(f)|^2 df} . \tag{3.29}$$

By appropriate derivation and normalization, using Rayleigh's theorem and Schwartz's inequality, the equation (3.29) can produce the following inequality:

$$\tau\beta \geq 1 . \tag{3.30}$$

This inequality defines a constraint between the signal bandwidth and the signal duration. The accuracy of range estimation is inversely proportional to the signal bandwidth. If the time bandwidth product of a signal is larger than 1, then the signal can thought as a "good" signal. In our sonar system, τ is about 0.005 ms and β is about 350 KHz, so the time bandwidth product is 1.75, which is larger than 1.

3.5 Summary

The outstanding performance of dolphin sonar inspires us to understand its physical principles and to try to apply them for underwater robotic systems. This chapter has described our system for trying to accomplish this. In the next chapter, we will discuss the performance of the system.

Chapter 4

Object Detection and Localization

Having described the binaural sonar sensing system in the previous chapter, we now proceed to assess the performance of the system. We first consider the accuracy of time-of-flight (TOF) estimation for individual sonar returns. Then, we assess the performance of using TOF measurements to estimate the range and angle to point objects. Finally, we consider the use of three TOF values to estimate object curvature.

4.1 Time of flight estimation

Echo detection plays a key role in the localization of objects. The time elapsed between the transmission and reception of the echo is used to determine the distance traveled by the sound wave. This enables us to estimate the position of an object. Time-of-flight estimation is the foundation of estimating the range and angle to an underwater object. We will discuss different detection methods in this section.

4.1.1 Simple threshold detector

In the simple threshold detection method, the amplitude of the detected signals is compared against a pre-set threshold level. When the signal amplitude first exceeds the threshold, the elapsed time from the transmission is recorded, which provides the traveling time.

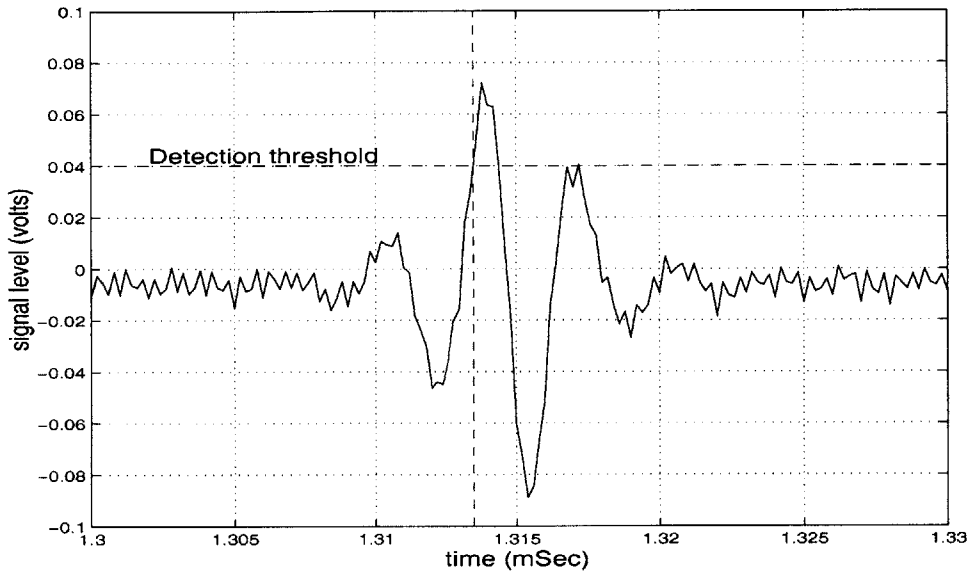

Figure 4-1: Illustration of simple threshold detector. The horizontal dashed line shows the amplitude threshold value (in this case, 0.04 volts). The vertical line shows the TOF value (in this case, 1.3135 milliseconds).

This method may lead to some errors, which are a consequence of the rise time of the waveform produced by the ultrasonic transducer. Actually, the received echo reaches the threshold level some time later than the exact beginning time of the echo, which creates an added delay. For the estimation of the range of a object, this disadvantage makes the target appear slightly farther away than it actually is. This error could be easily calibrated if the added delay is a constant. However, the amplitude of the echo is nondeterministic. There are many causes of echo amplitude variations which cannot be predicted, such as the size, the shape, the orientation and the materials of the target. For this reason, it is impossible to get a very accurate range estimate by a simple threshold method.

4.1.2 Energy detector

The energy detection method is similar to the simple threshold detection method. The difference is that the integrated energy is compared against the detection threshold, instead of just the simple amplitude value. The human auditory system is considered to use this kind of detector. Experiments have also indicated that the dolphin's inner ear functions like an energy detector [1]. Au et al. designed an experiment in 1988 to measure the integration time of the dolphin's energy detector for sonar pulses. They used a phantom target with electronically simulated echoes that could be controlled with high precision. Experiments showed that the integration time of the dolphin's sonar is about 264 msec. In order to realize an energy detector, we need to design a bank of contiguous filters and pass the echo signal through each filter bank. The filtered signal will be used to compare with the detection threshold. We did try this kind of energy detection method in our experiments. However, the detection accuracy is even worse than the simple amplitude detection method. It is well known that the dolphin's sonar has a high detection accuracy. So how the dolphin obtains this accuracy using the energy detection method is still a mystery that is worthy of future research.

4.1.3 Matched filter detector

The matched filter is an ideal receiver in the situation that the transmission signal is known and the background noise is white. Because it can produce the maximum SNR of the filter output, the matched filter is widely used and extremely important in radar and sonar signal processing.

We would like to explain why it is an optimal detector in two different ways:

1. Maximum likelihood estimation norm;
2. Maximum signal to noise ratio norm.

- **Maximum likelihood estimation**

  We express the event that the expected signal is present as:

$$H_1 : \tilde{\mathbf{r}} = \tilde{\mathbf{s}} + \tilde{\mathbf{n}}, \tag{4.1}$$

and the event that there is no signal is:

$$H_0 : \tilde{\mathbf{r}} = \tilde{\mathbf{n}}, \tag{4.2}$$

where the $\mathbf{r}$ and $\mathbf{n}$ are the signal and noise sampling vector, $\tilde{\mathbf{r}}$ and $\tilde{\mathbf{n}}$ are their complex envelope. So,

$$\begin{aligned} \tilde{\mathbf{r}}^T &= [\tilde{r}(t_1), \tilde{r}(t_2), ..., \tilde{r}(t_m)], \\ \tilde{\mathbf{s}}^T &= [\tilde{s}(t_1), \tilde{s}(t_2), ..., \tilde{s}(t_m)], \\ \tilde{\mathbf{n}}^T &= [\tilde{n}(t_1), \tilde{n}(t_2), ..., \tilde{n}(t_m)]. \end{aligned} \tag{4.3}$$

If we assume that $\tilde{\mathbf{n}}$ is Gaussian noise with zero mean and its covariance matrix is $\mathbf{R}_{\tilde{\mathbf{n}}}$ and $\tilde{\mathbf{s}}$ is a known signal, then the probability density distribution of the event H_1 is:

$$P_1(\tilde{\mathbf{r}}) = \frac{1}{(2\pi)^{\frac{m}{2}} |\mathbf{R}_{\tilde{\mathbf{n}}}|^{\frac{1}{2}}} exp[\frac{-(\tilde{\mathbf{r}} - \tilde{\mathbf{s}})^{*T} \cdot {\mathbf{R}_{\tilde{\mathbf{n}}}}^{-1} (\tilde{\mathbf{r}} - \tilde{\mathbf{s}})}{2}] \ . \tag{4.4}$$

Similarly, the probability density distribution of the event H_0 is:

$$P_0(\tilde{\mathbf{r}}) = \frac{1}{(2\pi)^{\frac{m}{2}} |\mathbf{R}_{\tilde{\mathbf{n}}}|^{\frac{1}{2}}} exp[\frac{-\tilde{\mathbf{r}}^{*T} {\mathbf{R}_{\tilde{\mathbf{n}}}}^{-1} \tilde{\mathbf{r}}}{2}] \ . \tag{4.5}$$

The likelihood function is:

$$\Lambda(\tilde{\mathbf{r}}) = exp[\frac{\tilde{\mathbf{r}}^{*T} {\mathbf{R}_{\tilde{\mathbf{n}}}}^{-1} \tilde{\mathbf{s}} + \tilde{\mathbf{s}}^{*T} {\mathbf{R}_{\tilde{\mathbf{n}}}}^{-1} \tilde{\mathbf{r}} - \tilde{\mathbf{s}}^{*T} {\mathbf{R}_{\tilde{\mathbf{n}}}}^{-1} \tilde{\mathbf{s}}}{2}] \ , \tag{4.6}$$

and

$$\ell(\tilde{\mathbf{r}}) = \ln \Lambda(\tilde{\mathbf{r}}) = -\tilde{\mathbf{s}}^{*T} {\mathbf{R}_{\tilde{\mathbf{n}}}}^{-1} \tilde{\mathbf{s}} + 2\tilde{\mathbf{r}}^{*T} {\mathbf{R}_{\tilde{\mathbf{n}}}}^{-1} \tilde{\mathbf{s}} + \mathbf{const} \ . \tag{4.7}$$

In the above equation, the first item $\tilde{\mathbf{s}}^{*T}\mathbf{R}_{\tilde{\mathbf{n}}}{}^{-1}\tilde{\mathbf{s}}$ and the **const** is irrelevant to $\tilde{\mathbf{r}}$, so we don't need to consider it. The decision equation is:

$$\tilde{\mathbf{r}}^{*T}\mathbf{R}_{\tilde{\mathbf{n}}}{}^{-1}\tilde{\mathbf{s}} \begin{matrix} (if\ H_1) > \\ (if\ H_0) < \end{matrix} \eta, \tag{4.8}$$

where η is the decision threshold. If all the noise samples are uncorrelated and their variances are equal, then can we normalize the covariance matrix $\mathbf{R}_{\tilde{\mathbf{n}}}$ as a unit matrix. So Equation (4.8) becomes:

$$e(t_m) = \tilde{\mathbf{r}}^{*T}\tilde{\mathbf{s}} = \sum_{i=1}^{m} \tilde{r}^*(t_i)\tilde{s}(t_i) \begin{matrix} (if\ H_1) > \\ (if\ H_0) < \end{matrix} \eta. \tag{4.9}$$

If we use the output of a filter to express Equation (4.9), that is,

$$e(t_m) = \sum_{i=1}^{m} h(t_m - t_i)\tilde{r}^{*T}(t_i)\ , \tag{4.10}$$

where $t_i = (i-1)\Delta t$ and Δt is sampling rate comparing equation (4.9) with equation (4.10), we get:

$$h(t_m - t_i) = \tilde{s}(t_i)\ . \tag{4.11}$$

That is,

$$h(t) = \tilde{s}(t_m - t)\ . \tag{4.12}$$

- **Maximum signal to noise ratio receiver**

  The meaning of Maximum signal to noise ratio receiver is how to find out a transfer function $H(jw)$ to make the SNR of the output of transfer network $h(t)$ maximum when the receiving signal is passed through this transfer function or filter. Assumed the background noise is white and its power spectrum density is:

$$P_{ni}(j\omega) = \frac{N_0}{2} \tag{4.13}$$

The frequency spectrum of input signal is:

$$\tilde{S}(j\omega) = \int_{-\infty}^{+\infty} \tilde{s}(t) e^{-j\omega t} dt \tag{4.14}$$

The output signal of the transfer network is:

$$\tilde{s}_0(t) = \frac{1}{2\pi} \int_{-\infty}^{+\infty} \tilde{S}(j\omega) H(j\omega) e^{j\omega t} d\omega \tag{4.15}$$

The average noise power at the output of the transfer network is:

$$\tilde{n}(t) = \frac{N_0}{4\pi} \int_{-\infty}^{+\infty} |H(\omega)|^2 d\omega \tag{4.16}$$

So, at the time t_m, the signal to noise ratio of the output of transfer network is:

$$(S/N)_{output} = \frac{|\tilde{s_0}(t_m)|^2}{n_0^2(t)} = \frac{|\frac{1}{2\pi} \int_{-\infty}^{+\infty} \tilde{S}(j\omega) H(j\omega) e^{j\omega t} d\omega|^2}{\frac{N_0}{4\pi} \int_{-\infty}^{+\infty} |H(\omega)|^2 d\omega} \tag{4.17}$$

Because,

$$|\int_{-\infty}^{+\infty} u(x) v(x) dx|^2 \leq \int_{-\infty}^{+\infty} |u(x)|^2 dx \cdot \int_{-\infty}^{+\infty} |v(x)|^2 dx \tag{4.18}$$

And we assume:

$$\begin{cases} u(\omega) &= \tilde{S}(j\omega) e^{j\omega t_m} \\ v(\omega) &= H(j\omega) \end{cases} \tag{4.19}$$

We substitute Equation (4.19) into Equation (4.18) and get:

$$|\frac{1}{2\pi} \int_{-\infty}^{+\infty} \tilde{S}(j\omega) H(j\omega) e^{j\omega t} d\omega|^2 \leq \frac{1}{4\pi^2} \int_{-\infty}^{+\infty} |H(\omega)|^2 d\omega \int_{-\infty}^{+\infty} |\tilde{S}(j\omega)|^2 d\omega \tag{4.20}$$

So combine the Equation (4.17) and Equation (4.20),

$$(S/N)_{output} \leq \frac{\frac{1}{4\pi^2}\int_{-\infty}^{+\infty}|H(\omega)|^2 d\omega \int_{-\infty}^{+\infty}|\tilde{S}(j\omega)|^2 d\omega}{\frac{N_0}{4\pi}\int_{-\infty}^{+\infty}|H(\omega)|^2 d\omega} \tag{4.21}$$

Or

$$(S/N)_{output} \leq \frac{\frac{1}{2\pi}\int_{-\infty}^{+\infty}|\tilde{S}(j\omega)|^2 d\omega}{\frac{N_0}{2}} = \frac{2E}{N_0} \tag{4.22}$$

where E is the total energy of input signal, given by:

$$E = \frac{1}{2\pi}\int_{-\infty}^{+\infty}|\tilde{S}(j\omega)|^2 d\omega \tag{4.23}$$

Equation (4.22) obtains its maximum value when

$$H(j\omega) = k\tilde{S}^*(j\omega)e^{-j\omega t_m}, \tag{4.24}$$

or

$$h(t) = k\tilde{s}(t_m - t), \tag{4.25}$$

K is a constant and we can normalize it as 1, then

$$h(t) = \tilde{s}(t_m - t). \tag{4.26}$$

Equation (4.26) is the same as equation (4.12). This processing method is called the matched filter. The matched filter is optimal when the detected signal is known and the noise is assumed to be additive, zero-mean, white and Gaussian. The details of implementing the matched filter are provided below.

4.1.4 Extended matched filter

The extended matched filter is a complement to the matched filter. It is used to detect a known signal in a colored noise background [20]. It has the following form:

$$H(j\omega) = \frac{S^*(\omega)e^{-j\omega T}}{S_n(\omega)}, \tag{4.27}$$

Where $S^*(\omega)$ is the conjugate of the frequency spectrum of the signal $s(t)$ and $S_n(\omega)$ is the spectrum density of color noise $n(t)$.

Comparing Equation (4.27) and Equation (4.24), we see that there is an additional denominator $S_n(\omega)$ in equation (4.27). It can be proven that the term $\frac{1}{S_n(\omega)}$ has the effect to whiten the colored noise. In practical applications, if there is no large variation in the noise frequency spectrum, the whitening process is not necessary. For example, in the underwater noise environment with a decay slope of 5 to 6 dB per octave, the whitening gain is less than 0.5 dB.

Figure 4-2 shows the frequency spectrum of the noise in our experiment tank when the equipment is in operation. We think the matched filter is enough for echo processing in our experiments.

4.1.5 Implementation of matched filter

Generally, there are three steps included in the implementation of the matched filter:

- **Choosing a template representation**

  The matched filter assumes that the detected signal is known to implement the matched filter we first have to choose a template for the echo signal. In the situation that the object is close to the sonar system, the echo signal can be assumed to be proportional to the transmitted signal as we have discussed in Chapter 3. So we can choose the transmission signal as a template. However, for our sonar system, the fixed transducer frequency response and the only pulse modulation method in our power-amplifier impose a limit of this freedom. Basically, a good transmission signal should have a sharp main lobe and low side lobe. A sharp main lobe will increase range resolution and a low side lobe can be helpful to decrease ambiguity. Another advantage of low side lobe is that it can increase the detection accuracy in the multi-echoes situation.

- **Calculating the matched filter**

  The matched filter calculation calculates the correlation between the template signal and the received signal $h(t)$ is described in this earlier section. We can

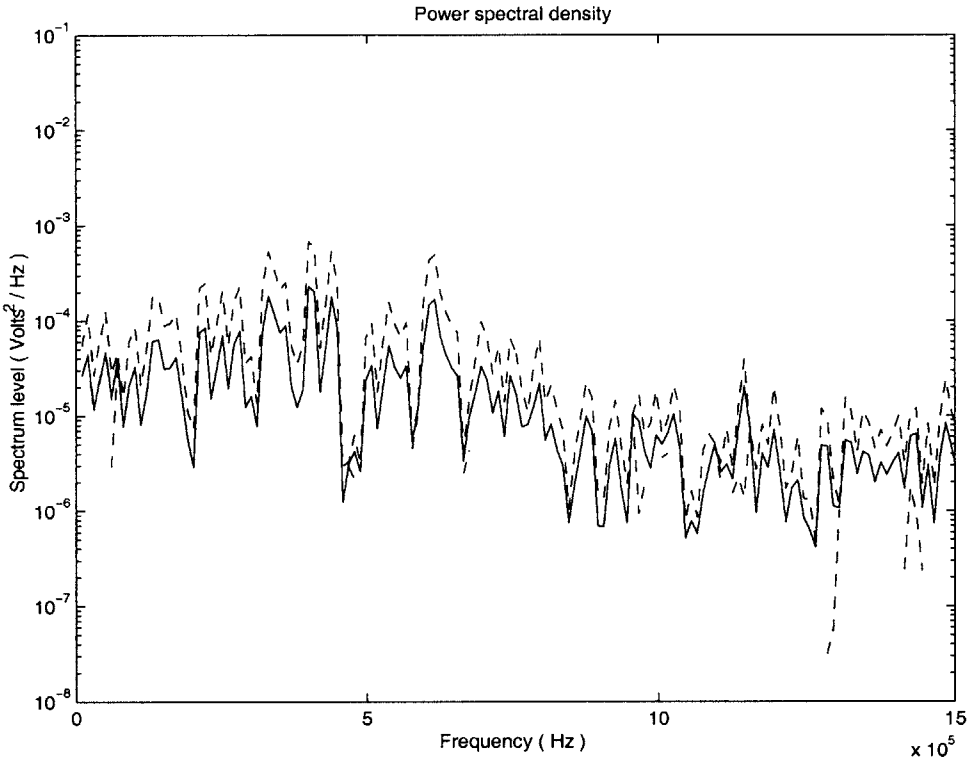

Figure 4-2: The frequency spectrum of the noise in the tank. The dash lines show the 95% confidence interval of spectrum estimation. We can see that there is not much variation in the spectrum. In consideration of the indetermination of the noise and the less filtering gain at the expense of computation complexity of extended filter, we think the matched filter is enough for echo detection in tank.

conveniently utilize the matlab function xcorr to implement it while it may be more complex if using other language.

- **Peak detection**

  Determining the peak points in the signal at the output of the matched filter is the final step to obtain a TOF estimate with the matched filter detector. If only one object is present in the active operation region, signal echo will be acquired at the receiver. We should only find out the global maximum point of the filtered echo signal. If there are multi-objects located in the sonar operation space, multi-echoes will be captured. They construct a linear combinations in the receiving signal. To detect them, multiple local peak points should be picked up. This cab be more complex with additional considerations of side-lobe affect. In our experiment we will discuss later, there is only single point object or curvature object assumed to contribute the echo in the receiving signal. When the peak has been detected after matched filtering, the TOF value of the echo will be determined in the receiving signal according to the time shift of the peak at the output of the matched filter. This can be understood from Figure 4-3.

4.2 Localization of point objects

Having introduced the different signal detection methods and how to implement them, in this section we will introduce how to use them in practical applications.

4.2.1 Methods

The beam angles of the transmitter and the receivers of the biomimetic sonar determine an active region. Only within the active region can an obstacle be detected. We assume that there is a target in the active region with polar coordinates r and θ. The TOF information of the two receivers, TOF_1 and TOF_2, can be obtained by properly detecting the echo signal with the simple amplitude detection method and the matched filter detection method:

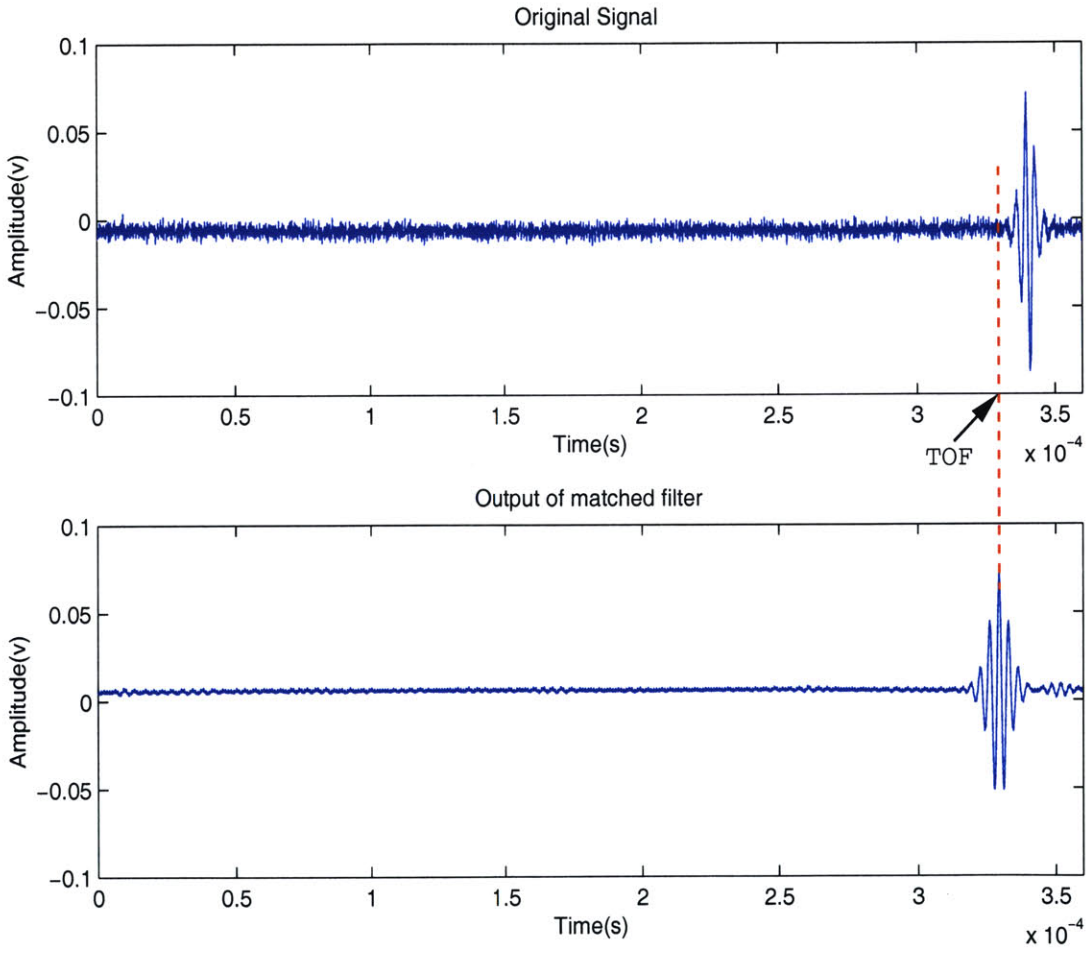

Figure 4-3: Illustration of TOF estimation by using a matched filter.

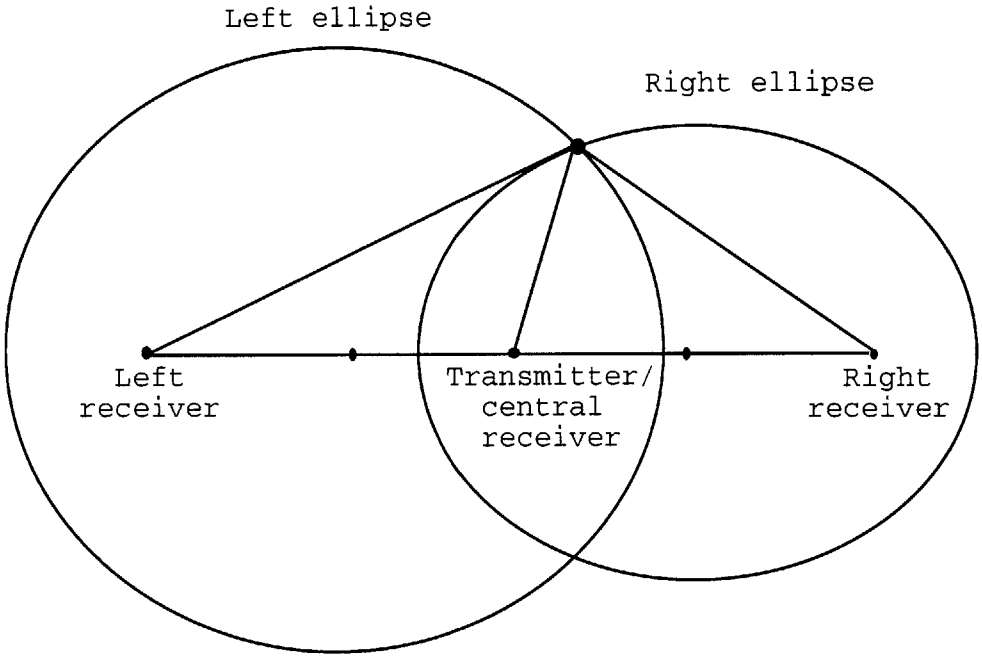

Figure 4-4: Illustration of the intersection of two ellipses. A point object is at the intersection of the two ellipses defined by the sound travel path.

$$\begin{aligned} R_1 &= c \times TOF_1 \ , \\ R_2 &= c \times TOF_2 \ , \end{aligned} \tag{4.28}$$

where c is the underwater sound speed, R_1 defines a possible target contour which is an ellipse with foci on the transmitter and receiver 1, and R_2 defines a possible target contour which is an ellipse with foci on the transmitter and receiver 2.

The intersection of the two ellipses determines the location of an underwater point target, as shown in Figure 4-4.

The geometrical relation between the object and the biomimetic sonar is illus-

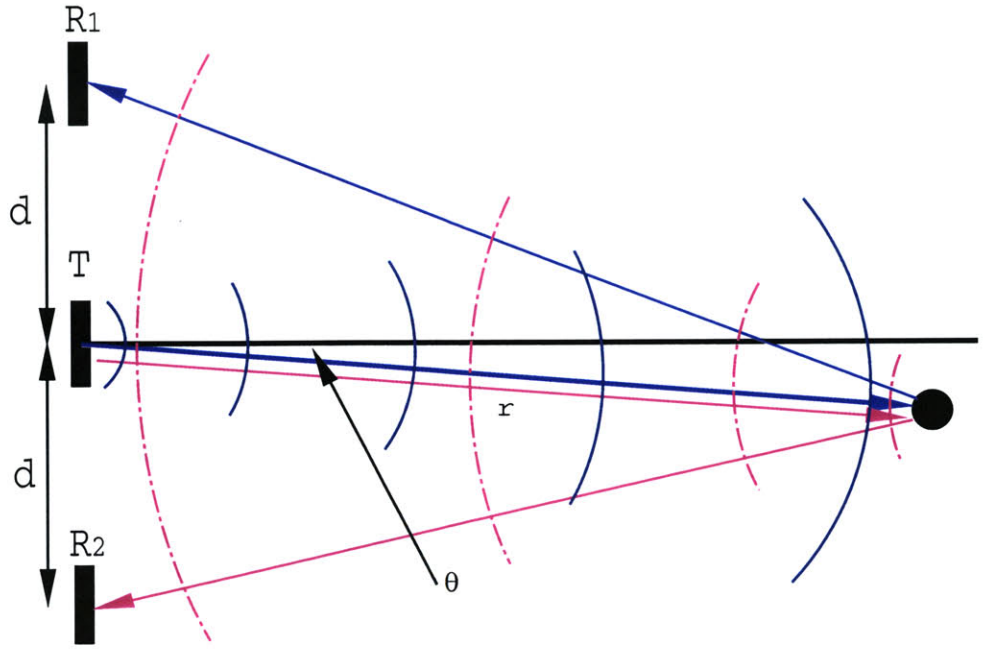

Figure 4-5: Geometry of echolocation for a point target. The figure shows the transmitter and two receivers at the left, which are separated by the distance d. The measured travel times for the sound paths from the transmitter to the two receivers are used to estimated the range and bearing to the target.

trated in Figure 4-5, from which we can obtain:

$$\begin{aligned} R_1 &= \sqrt{r^2 + d^2 + 2rd\sin\theta} + r, \\ R_2 &= \sqrt{r^2 + d^2 - 2rd\sin\theta} + r. \end{aligned} \tag{4.29}$$

Solving Equation (4.29), we can get:

$$r = \frac{R_1^2 + R_2^2 - 2d^2}{2(R_1 + R_2)}\ , \tag{4.30}$$

and

$$\theta = \arcsin\frac{(R_1R_2 + d^2)(R_1 - R_2)}{d(R_1R_2 - 2d^2)}\ , \tag{4.31}$$

where r and θ define the location of the object.

4.2.2 Simulation

By using simulations, we hope to obtain a brief understanding of how well the matched filter and simple threshold detector work by comparing their performance in localization of a point object.

According to Barshan and Kuc [6], the sound pressure in the free sound field space can be described as:

$$P(r,\theta) = \frac{P_0}{r} \cdot e^{-\frac{2\theta^2}{\theta_0^2}} , \tag{4.32}$$

where θ_0 is the half width angle of transducer.

According to Equation (4.32), we can simulate the sound pressure amplitude at the receivers from the object with different r and θ . In order to mimic the configuration of dolphin's sonar, we consider the receiver as omni-directional receiver. In simulation, the time delay of the echo can be obtained by calculating the real distance from the transducers to the object. A random noise is added to the signal to simulate a noisy environment.

All the simulation results are shown from Figures 4-6 to Figure 4-11. These results illustrate the strength of the matched filter, especially when the echo signal has a low SNR.

4.2.3 Experiment

Although the simulations have demonstrated the advantage of the matched filter and we have made a comparison of the localization performance by using the two detection methods, experiments are essential to verify our analysis. To determine the performance of our biomimetic binaural sonar system, an experiment was set up in the M.I.T. marine instrumentation and computation laboratory.

The sharp edge of a triangle was modeled as an point object in the experiment. Although there may be a small difference between the echo signal between a sharp edge and a point object, we assume that this difference can be neglected. First, we fixed the angle and varied the range of the sonar system from 0.1 meters to 2.5 meters

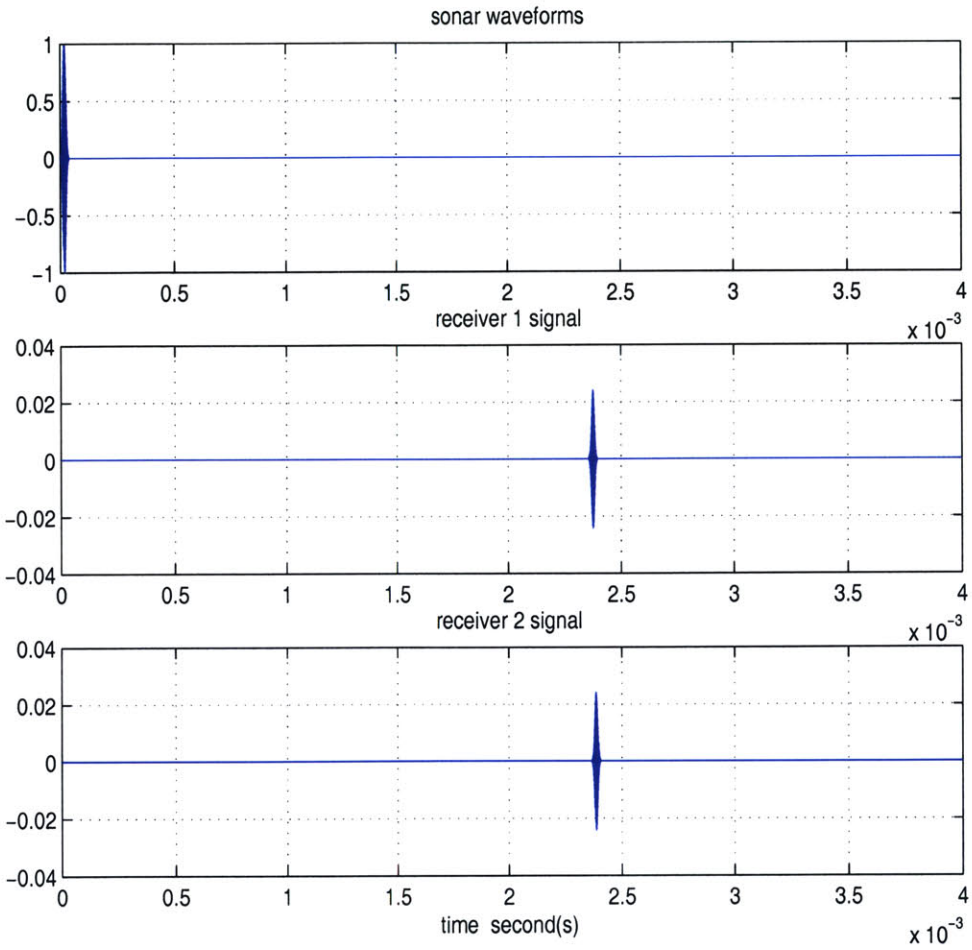

Figure 4-6: Transmitted and received signals for a situation with high SNR. The top plot shows the transmitted signal. The bottom two plots show the received signals for the left and right receiver transducers. For this scenario, the inclination angle between the transmitter and object is about 2.2 degrees and the range is about 1.8 m.

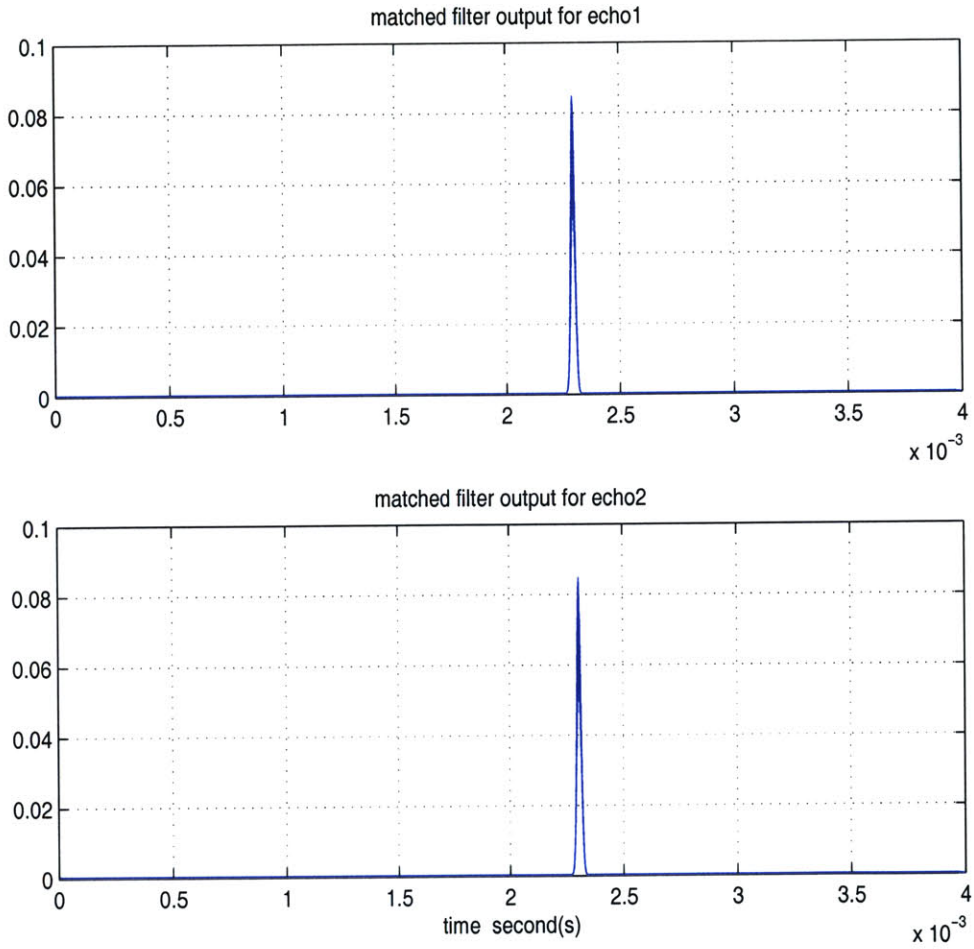

Figure 4-7: Matched filter outputs for the two echo signals shown in Figure 4-6.

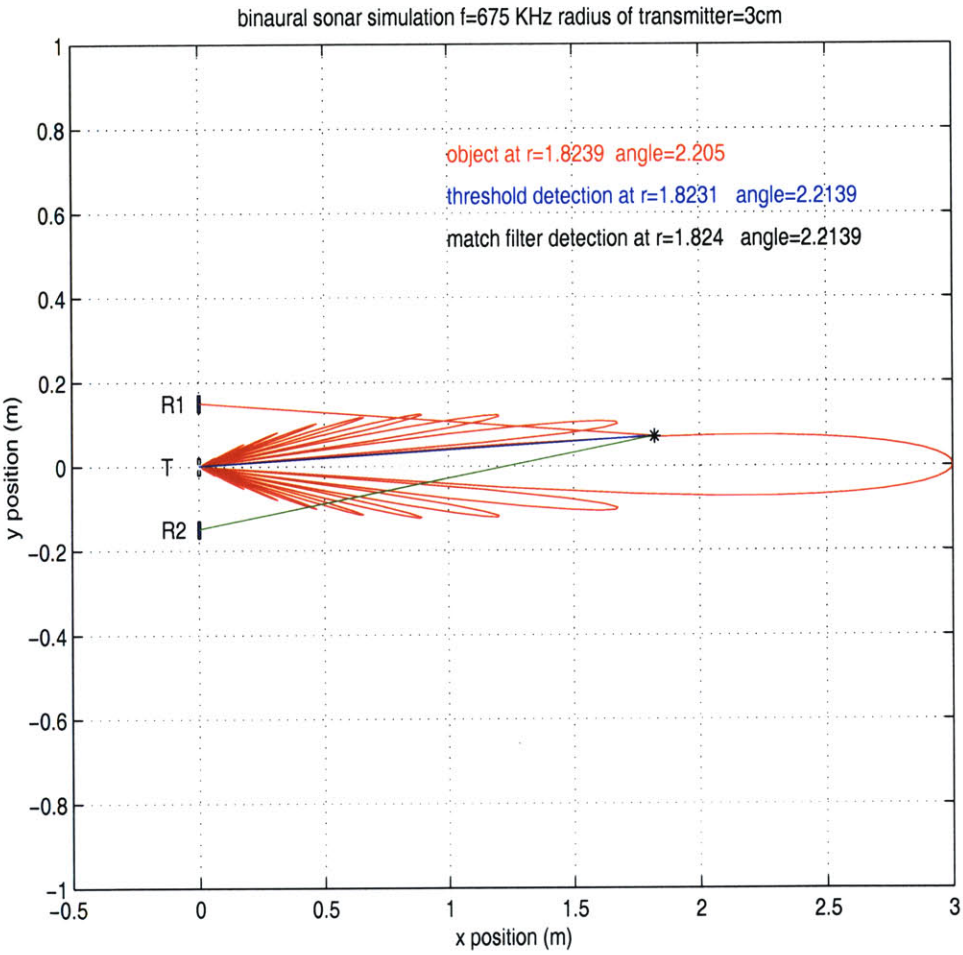

Figure 4-8: Illustration of detection results for a situation with high SNR. The estimated locations of the objects from these two methods coincide.

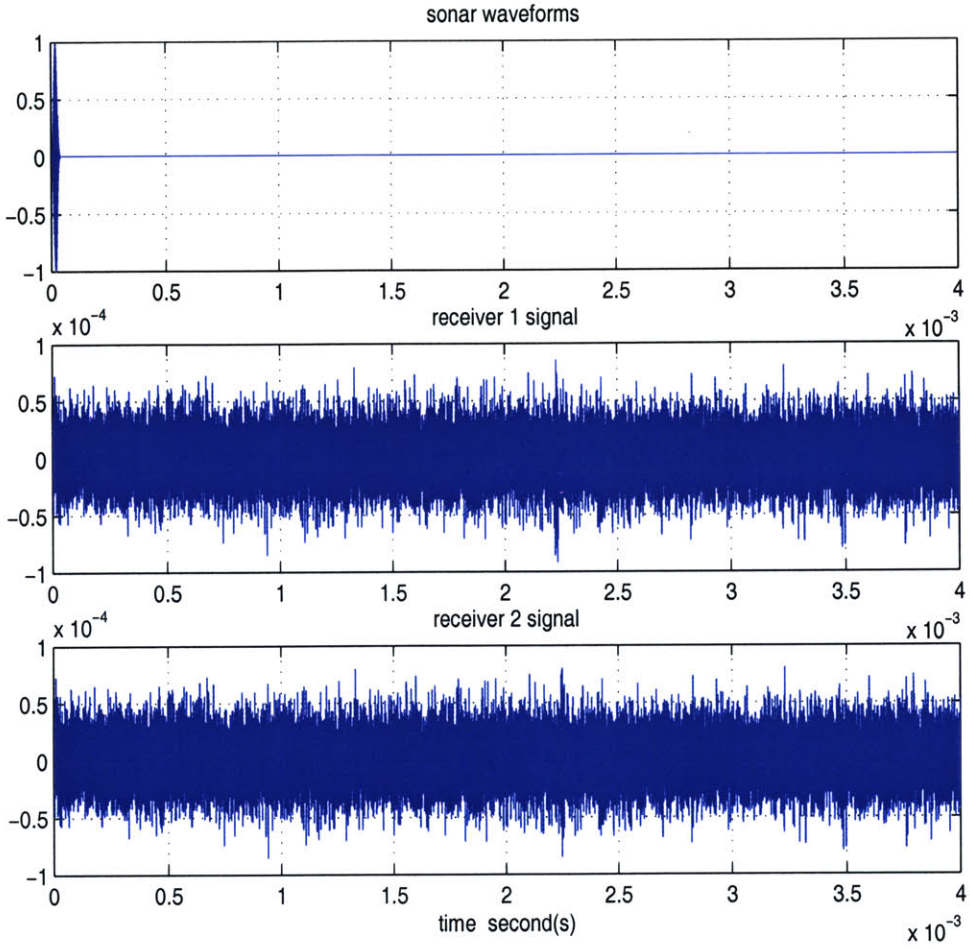

Figure 4-9: Transmitted and received signals for a situation with low SNR. The top plot shows the transmitted signal. The bottom two plots show the received signals for the left and right receiver transducers, with a very high noise level.

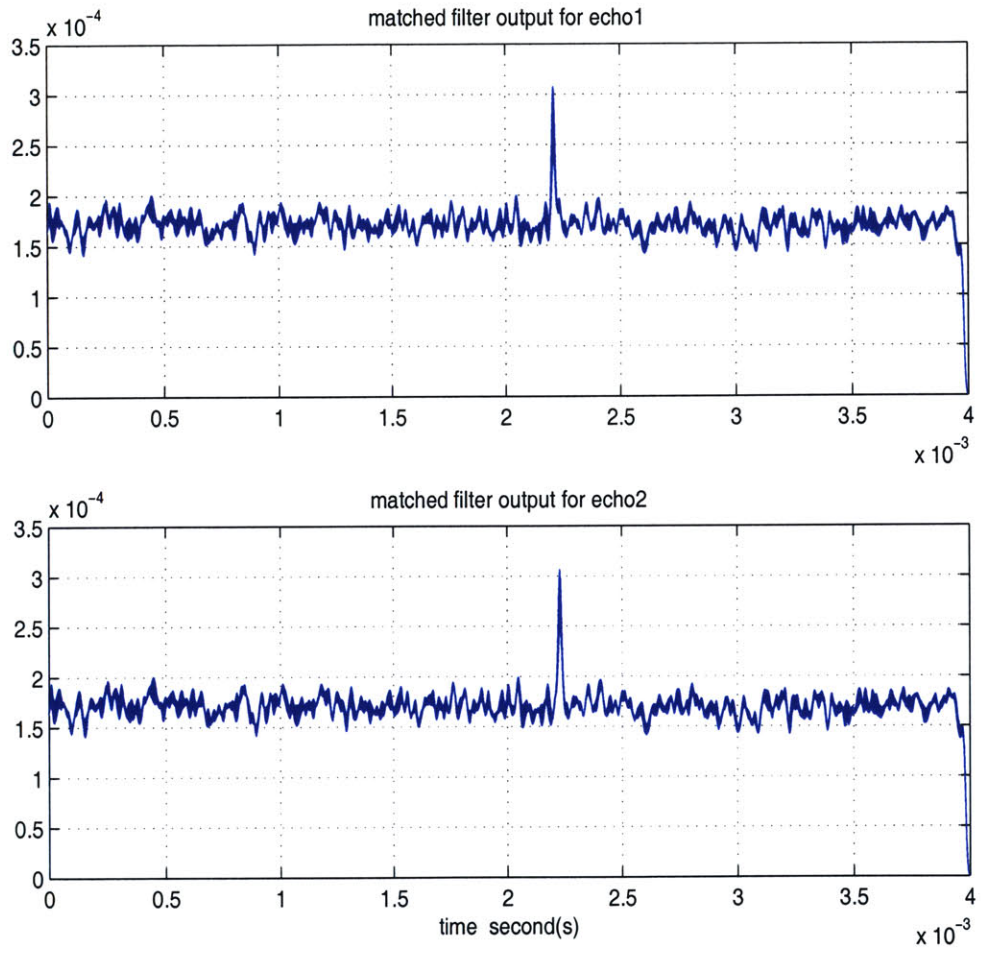

Figure 4-10: Matched filter outputs for the two received signals shown in Figure 4-9.

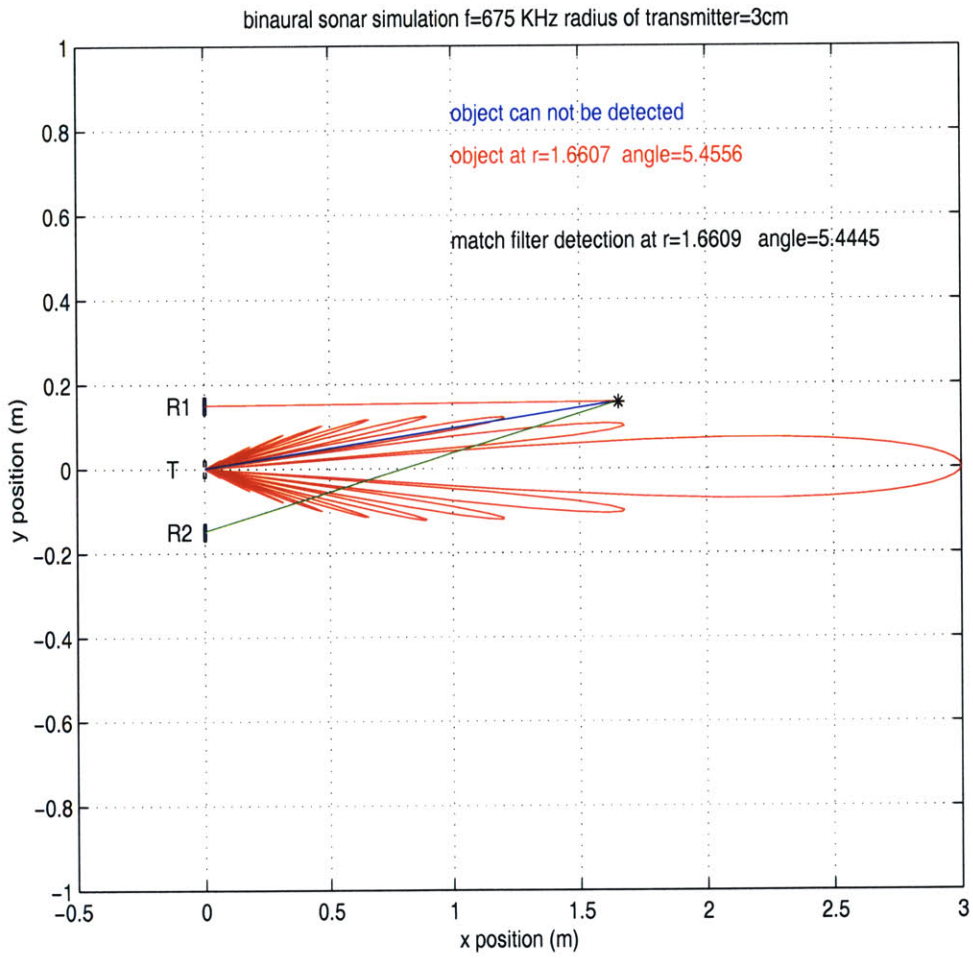

Figure 4-11: Detection results for a situation with low SNR. The object could not be detected by the simple threshold detector, but the matched filter detector still works well. The estimation location of the object is very close to the real location.

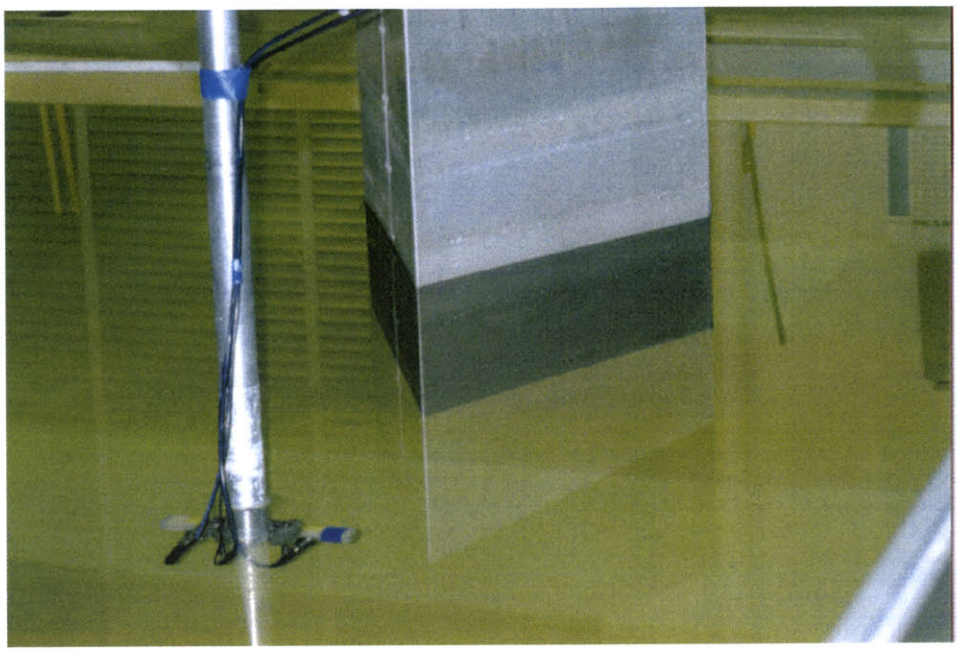

Figure 4-12: Experiment setup.

in 0.1 meter increments. Second, we fixed the range and changed the angle of the sonar from $-12°$ to $12°$ in $1°$ increments. The object is assumed static.

For each transmitted pulse, the two receivers captured two echo signals. At every location that the biomimetic sonar moves to, 50 sample echo signals were collected and averaged. The two TOFs were obtained by employing a simple threshold detector and a matched filter detector. Using Equation (4.30) and Equation (4.31), the range and angle of the underwater point target have been estimated by employing both methods of TOF estimation. The estimation results are shown in Figure 4-13 and Figure 4-14.

In Figure 4-13, the angle of the biomimetic sonar was fixed, only the range of the biomimetic sonar was changed and estimated, to determine the relationship between the estimation error and range. From these results, we can determine:

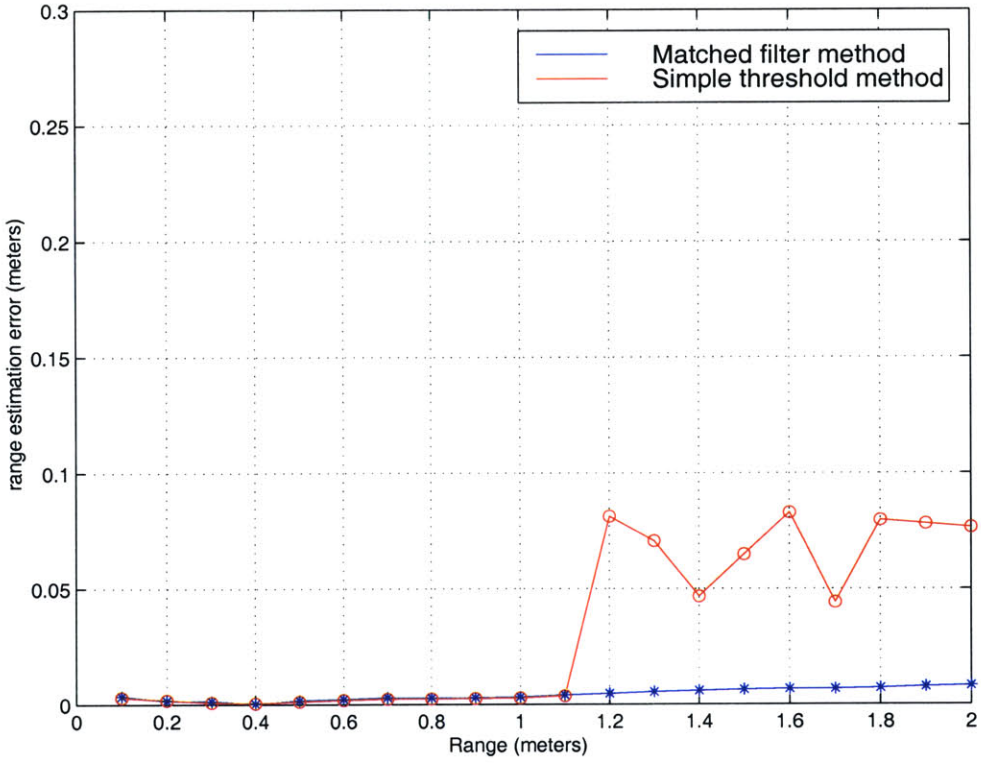

Figure 4-13: Range estimation error as a function of range. The computation time for threshold detection was 0.008 seconds at each position and the computation time for matched filtering was 0.866 seconds at each position.

1. The estimation error of both the simple threshold method and matched filter method increases as the range increases.

2. The maximum estimation error of the matched filter method is within 0.01 meters and the maximum estimation error of the simple threshold method is within 0.08 meters.

3. When the biomimetic sonar is close to the underwater target (range < 1 m), the echo signal has a better SNR, and the estimation effects of the simple threshold detector and matched detector are very close. However, as the SNR decreases, the matched filter does much better.

4. The average estimation time of the matched filter method is much larger than the average estimation time of the simple threshold method.

In Figure 4-14, the range of the biomimetic sonar was fixed and the angle to the target was estimated for different angles of the sonar. From these results, we can determine:

1. The estimation error of both the simple threshold method and the matched filter increase with angle of incidence.

2. The maximum estimation error of the matched filter method is within $0.2°$ and the maximum estimation error of the threshold method is within $0.6°$.

3. When the inclination angle between the biomimetic sonar and the underwater point target is small (angle $< 3°$), the echo signals have a better SNR, and the estimation results of the threshold detector and the matched filter detector are very close. However, when the inclination angle becomes large, the estimation error of the threshold method increases, and at a certain point the object can not even be detected. The angle estimation error is very sensitive to the angle of incidence.

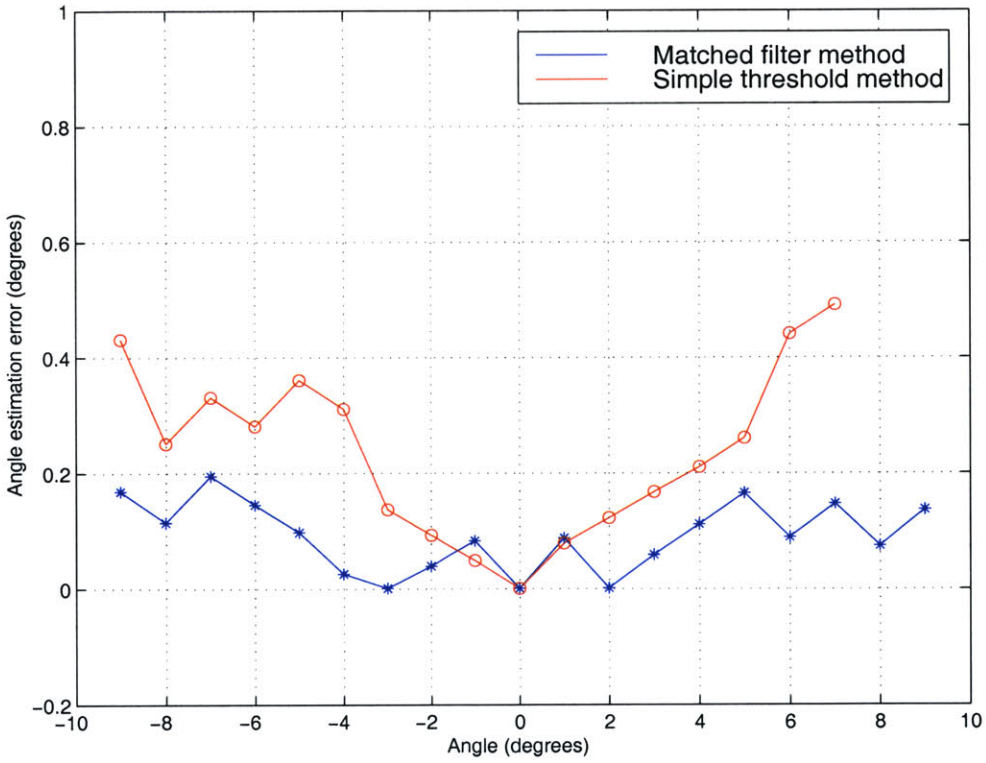

Figure 4-14: Angle estimation error as a function of angle of incidence. The computation time for threshold detection was 0.007 seconds at each position and the computation time for matched filtering was 0.838 seconds at each position.

4.2.4 Improved echo processing

This section describes some alternate processing techniques that were evaluated to reduce the effects of noise and to save processing time. In the practical applications of an underwater robot sonar system, the detection accuracy and detection time are always two major considerations. Generally, the detection accuracy and the detection time play two contradictory roles. That is, the improvement of detection is often at the expense of detection time and vice versa. Besides the simple threshold detector and matched filter we have mentioned before, other possible methods for data post-processing are processing of averaged waveforms and band-pass filtering.

By processing the average of several different signals of the same scene, the effect of white noise can be reduced dramatically. This can be described as:

$$X = \sum_{i=1}^{N} \frac{x_i}{N}, \tag{4.33}$$

where, x_i is the i th echo signal sample collected at the same location by sonar and N is the total number of signals.

A band-pass filter is designed according to the center frequency and the bandwidth of the desired passing signal. It can increase the SNR by filtering unfavorable noise that is out of the frequency band of the signal of interest.

In addition to the simple threshold detector and the matched filter detector, the following combinations were experimented with:

1. simple threshold detection on a single waveform;
2. simple threshold detection on an average waveform;
3. matched filter detection on a single waveform;
4. matched filter detection on an average waveform;
5. simple threshold detection on a bandpass filtered single waveform;
6. simple threshold detection on a bandpass filtered average waveform;

7. matched filter detection on a bandpass filtered single waveform;

8. matched filter detection on a bandpass filtered average waveform;

9. local matched processing method.

The last combination, referred to above as "local matched processing method", is described in more detail below. To investigate the processing effect of these combinations, we collected 68 pings of data captured using the binaural sonar at a range from 2 m to 5 m. The processing time and correct detection rate for the different scenarios are shown below. A detection is considered correct if the range estimation error is less than 1 cm.

From Figure 4-15 through Figure 4-17, we can clearly see that a higher correct detection rate means a greater detection time. No method can satisfy the requirements of saving processing time while keeping reasonable detection accuracy. Also, the matched filter is the major factor in increasing both the detection accuracy and time expense. The averaging process and the bandpass filter do not contribute much in processing time but are beneficial for improvement of detection accuracy.

A natural thought is to ask, " can we reduce the matched filter processing time? ". Noticing that a complete echo signal is required for matched processing, we propose a local matched processing method. First, the peak point of the echo signal is detected. Then, a local matching process is executed between a known template signal and the partial echo signal which is around the detected peak point. The time duration of the partial echo signal is about twice of that of the template signal. By finding the peak of the output of the local matched filter and carefully calibrating the offset caused by defining the partial echo signal, an accurate time-of-flight estimate can be determined.

We call this method a local matched processing method. The comparison between the methods is shown in Figures 4-15 to Figure 4-17. It can be easily seen that the local matched processing method provides an improvement in detection rate with much less computation time.

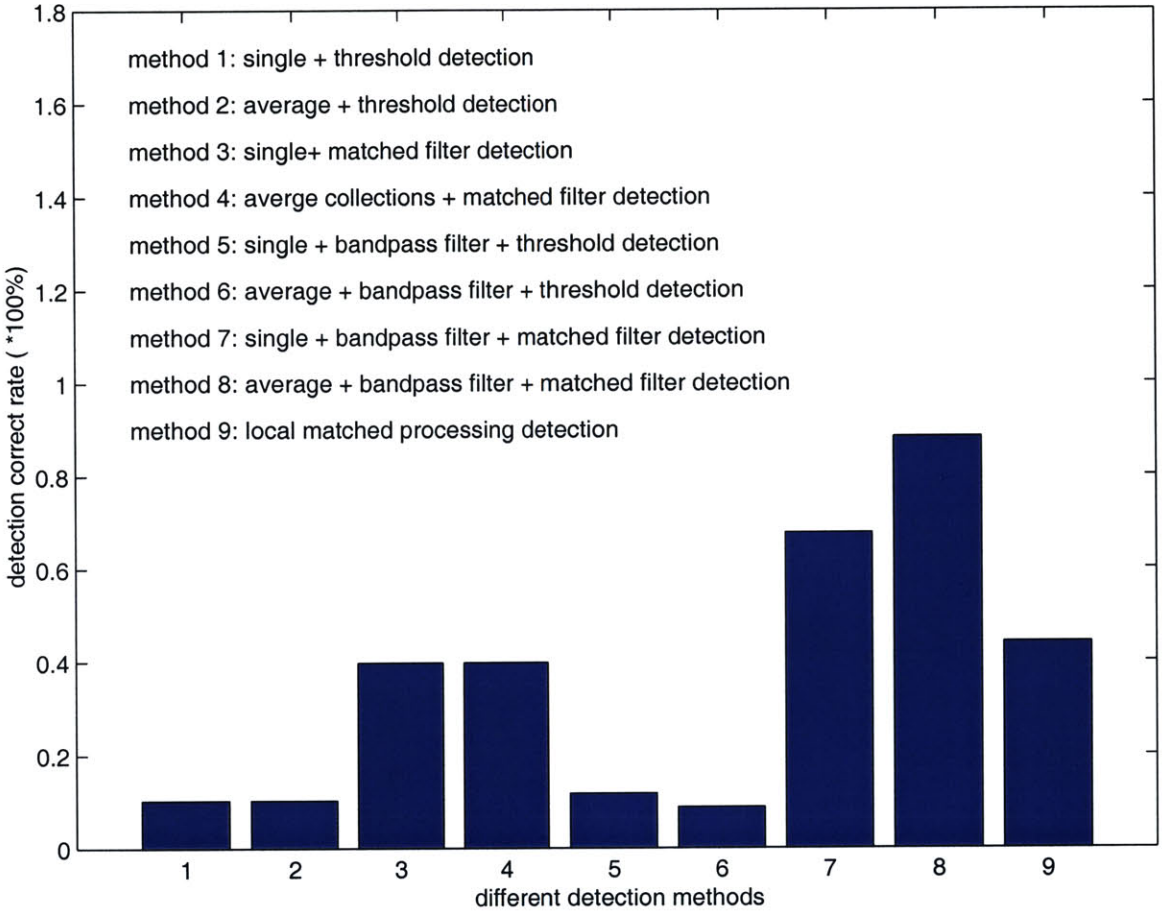

Figure 4-15: A comparison of correct detection rate using the nine different detection methods.

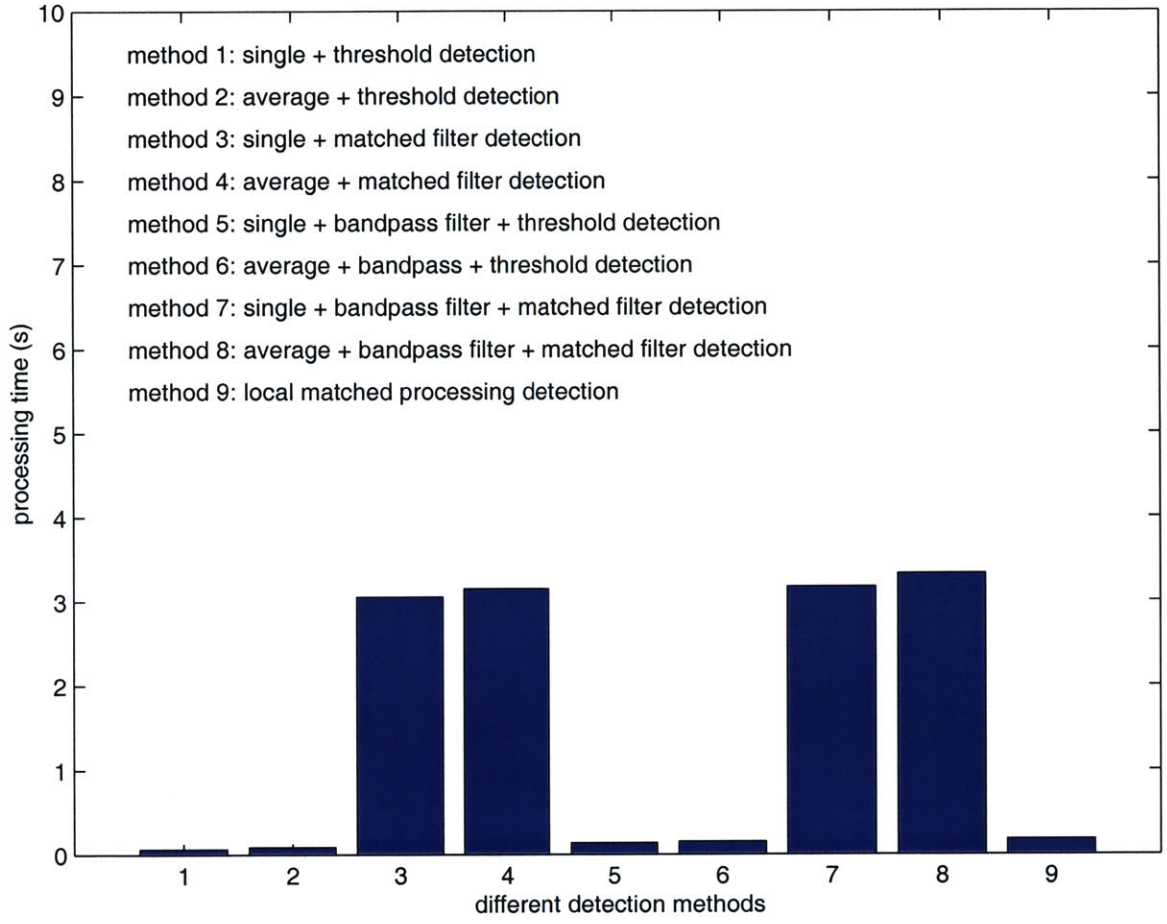

Figure 4-16: A comparison of processing time using the nine different detection methods.

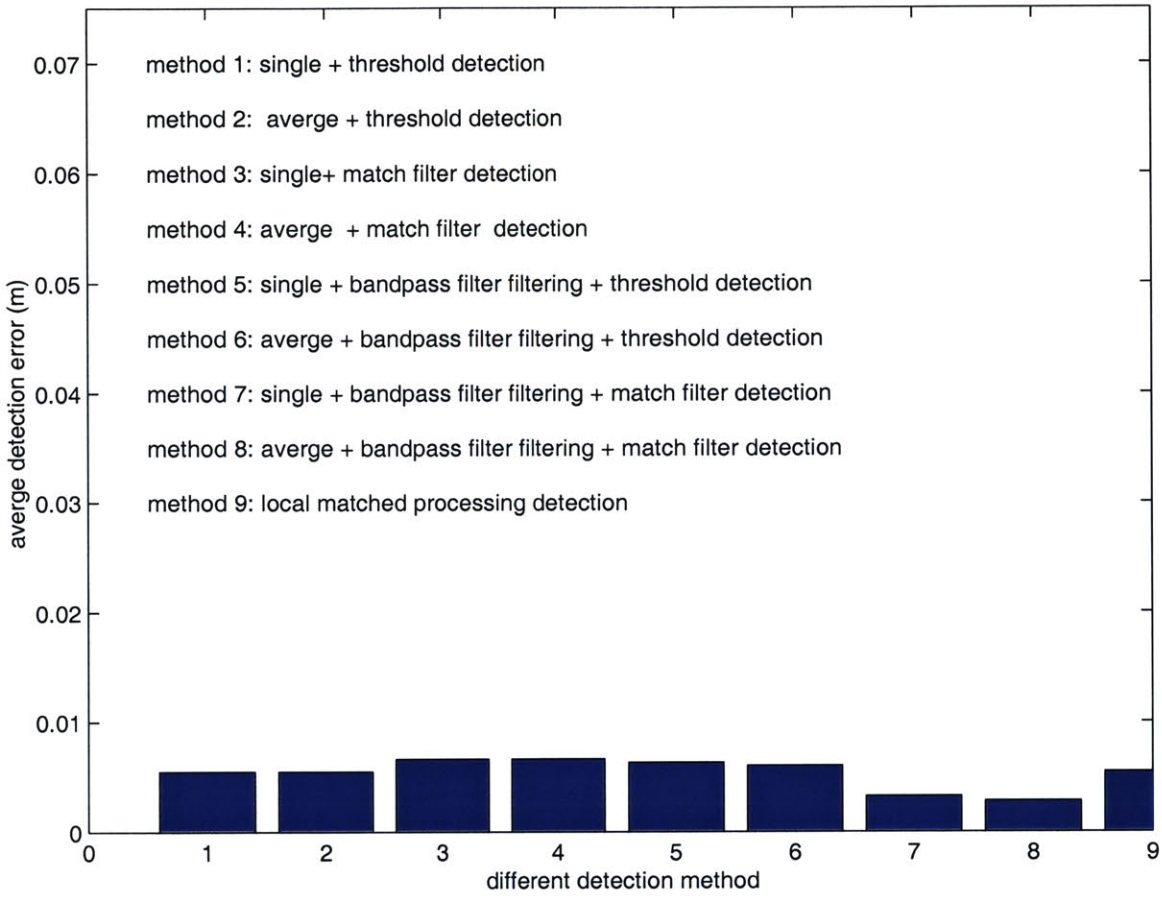

Figure 4-17: A comparison of detection error using the nine different detection methods.

4.3 Curvature estimation

4.3.1 Methods

In the underwater world, the objects and terrain can be very complex $3D$ shapes. The development of methods to handle very complex objects is a critical area for future research. Hence, we consider one small step in this direction by considering how to localize $2D$ cylindrical objects. Plane objects and point object can also be modeled as curved objects with a radius of $R_{plane} = \infty$ and $R_{point} = 0$.

Inspired by the idea that the center transmitter of our sonar system can also act as a receiver, we rearrange the configuration of the sonar system as a tri-aural sensor system as Peremans [34] has done. Three transducers are necessary to estimate curvature from a single ping. We have implemented two methods for estimating curvature. One is an approximate analytical solution, which was published by Peremans. The other is a numerical solution, which to our knowledge has not been implemented before.

Method 1: Approximate solution

According to the definition of an ellipse and the physics of sound transmission, the problem of localizing a cylindrical underwater object is equivalent to determining a circle which is tangent to two ellipses and one circle as shown in Figure 4-18.

The definitions in Figure 4-18 are:

$$left\ ellipse : \frac{(x - \frac{d}{2})^2}{(\frac{M_l}{2})^2} + \frac{y^2}{(\frac{M_l}{2})^2 - (\frac{d}{2})^2} = 1 \ , \tag{4.34}$$

$$center\ cycle : x^2 + y^2 = (\frac{M_c}{2})^2 \ , \tag{4.35}$$

$$right\ ellipse : \frac{(x - \frac{d}{2})^2}{(\frac{M_r}{2})^2} + \frac{y^2}{(\frac{M_r}{2})^2 - (\frac{d}{2})^2} = 1 \ , \tag{4.36}$$

where, M_l is the estimated sound travel distance from the center transmitter to the left receiver, M_r is the estimated sound travel distance from the center transmitter to the

right receiver, M_c is the estimated sound travel distance from the center transmitter to the center receiver/transmitter, and d is the separation between the transmitter and receivers.

The foci of these ellipses are located at the three transducers. The center of the circle is at the transmitter. Directly finding out the location of the expected reflecting object, for example, a tangent cylinder here, from the above Equations (4.34), (4.35), and (4.36) is very difficult. When the measurements M_l, M_r are all much larger than the separation d, we can assume the left ellipse and the right ellipse are circles with radius:

$$R_{left} = r_1 = \frac{\sqrt{M_l^2 - d^2}}{2} , \tag{4.37}$$

and

$$R_{right} = r_3 = \frac{\sqrt{M_r^2 - d^2}}{2} . \tag{4.38}$$

This is illustrated in Figure 4-19.

From the geometric relationship shown in Figure 4-19, we have:

$$x_c^2 + y_c^2 = (r_c + r_2)^2, \tag{4.39}$$

$$(x_c + \frac{d}{2})^2 + y_c^2 = (r_c + r_1)^2, \tag{4.40}$$

and

$$(x_c - \frac{d}{2})^2 + y_c^2 = (r_c + r_3)^2. \tag{4.41}$$

Solving Equations (4.37) to (4.41), we obtain [34]:

$$r_c = \frac{r_1^2 + r_3^2 - 2r_2^2 - \frac{d^2}{2}}{4r_2 - 2r_1 - 2r_3} , \tag{4.42}$$

$$x_c = \frac{(r_1 - r_3) \cdot (2r_c + r_1 + r_3)}{2d} , \tag{4.43}$$

and

$$y_c = [(r_c + r_2)^2 - x_c^2]^{\frac{1}{2}} . \tag{4.44}$$

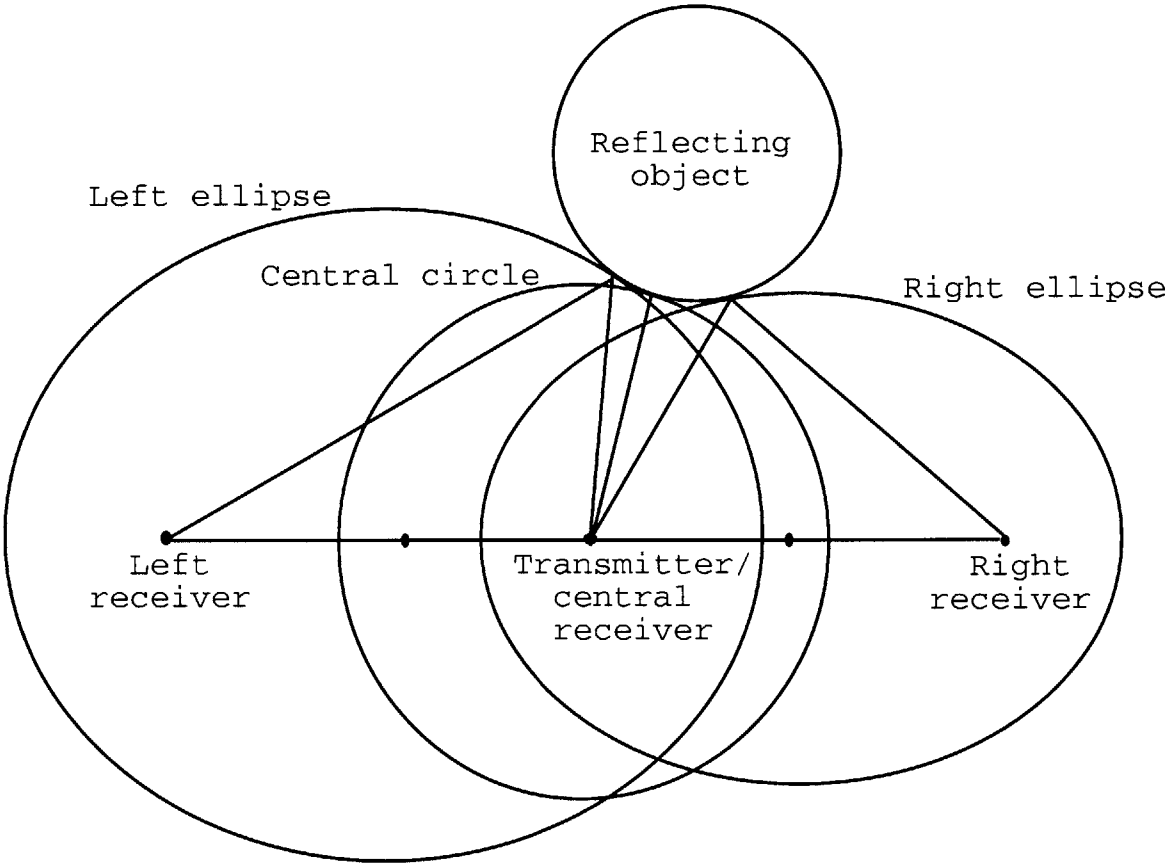

Figure 4-18: Illustration of ellipse and circle constraints. The reflecting object is tangent to the ellipses and circles defined by sound travel path.

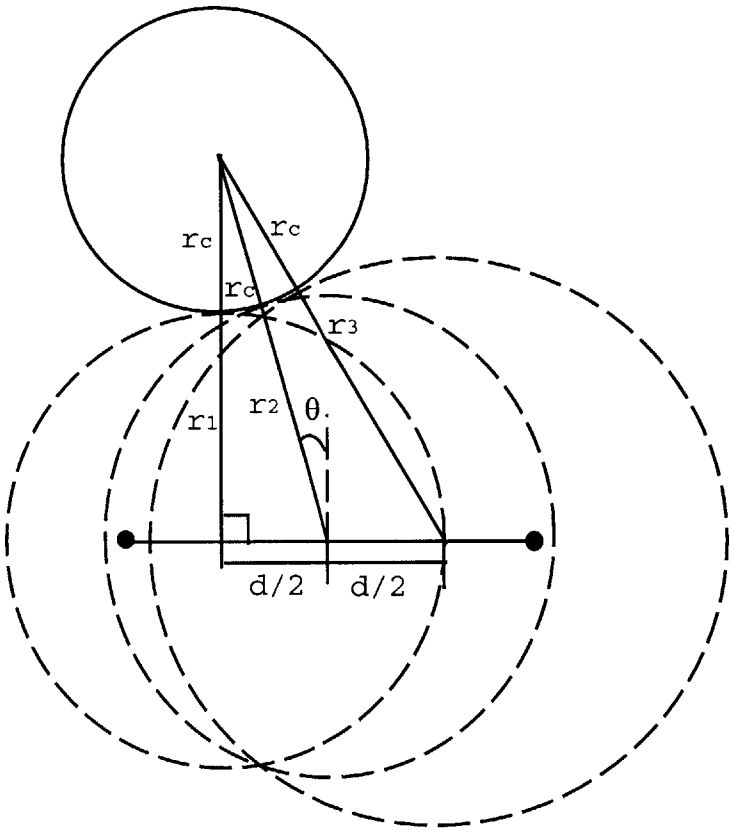

Figure 4-19: Approximation of Figure 4-18. The left and the right ellipses can be assumed as circles when the sound travel paths are much larger than the separation between the transducers. The radius of the circles are equal to the minor axis of the ellipses.

Although the approximations above may be reasonable and the expression in Equations (4.42), (4.43), and (4.44) is very simple, the approach has some difficulties. As discussed by Peremans, noise sensitivity is a serious concern with this approach.

Method 2. Numerical solution incorporating elliptical constraints

Figure 4-20 shows a complete geometric relationship regarding the reflection between a tri-aural sonar and a cylinder reflector.

We have 4 known parameters, d, M_l, M_r and M_c. M_l, M_r and M_c represent the estimations of the sound travel distance at the three receivers and d is the separation between transducers. The location and the radius of the cylinder reflector are given by: x_c, y_c, and r_c . The other unknown parameters are: x_r, y_r, x_m, y_m, x_l, y_l, d_1, and d_2 . The (x_c, y_c), (x_r, y_r) and (x_l, y_l) are the exact reflecting points at the cylinder from the sound transmission to the center, right and left transducers, respectively. The distances d_1 and d_2 are illustrated in Figure 4-20.

For the transmission from the center transmitter **T** to the receiver **R1**, $\alpha = \beta$, so we have:

$$d_1 \cdot \sqrt{(x_r - d)^2 + y_r^2} = (d - d_1) \cdot \sqrt{x_r^2 + y_r^2} \ . \tag{4.45}$$

Due to the straight line constraint [from *(Xc, Yc)* to *(Xr, Yr)* to *(0, d1)*], we have:

$$(x_c - d_1) \cdot y_r = (x_r - d_1) \cdot y_c \ . \tag{4.46}$$

Due to the circle constraint, we have:

$$(x_c - x_r)^2 + (y_c - y_r)^2 = r_c^2 \ . \tag{4.47}$$

From the estimation of the sound travel distance, we have:

$$\sqrt{x_r^2 - y_r^2} + \sqrt{(x_r - d)^2 + y_r^2} = M_r \ . \tag{4.48}$$

Similarly, for the transmission from the center transmitter **T** to the receiver **R2**,

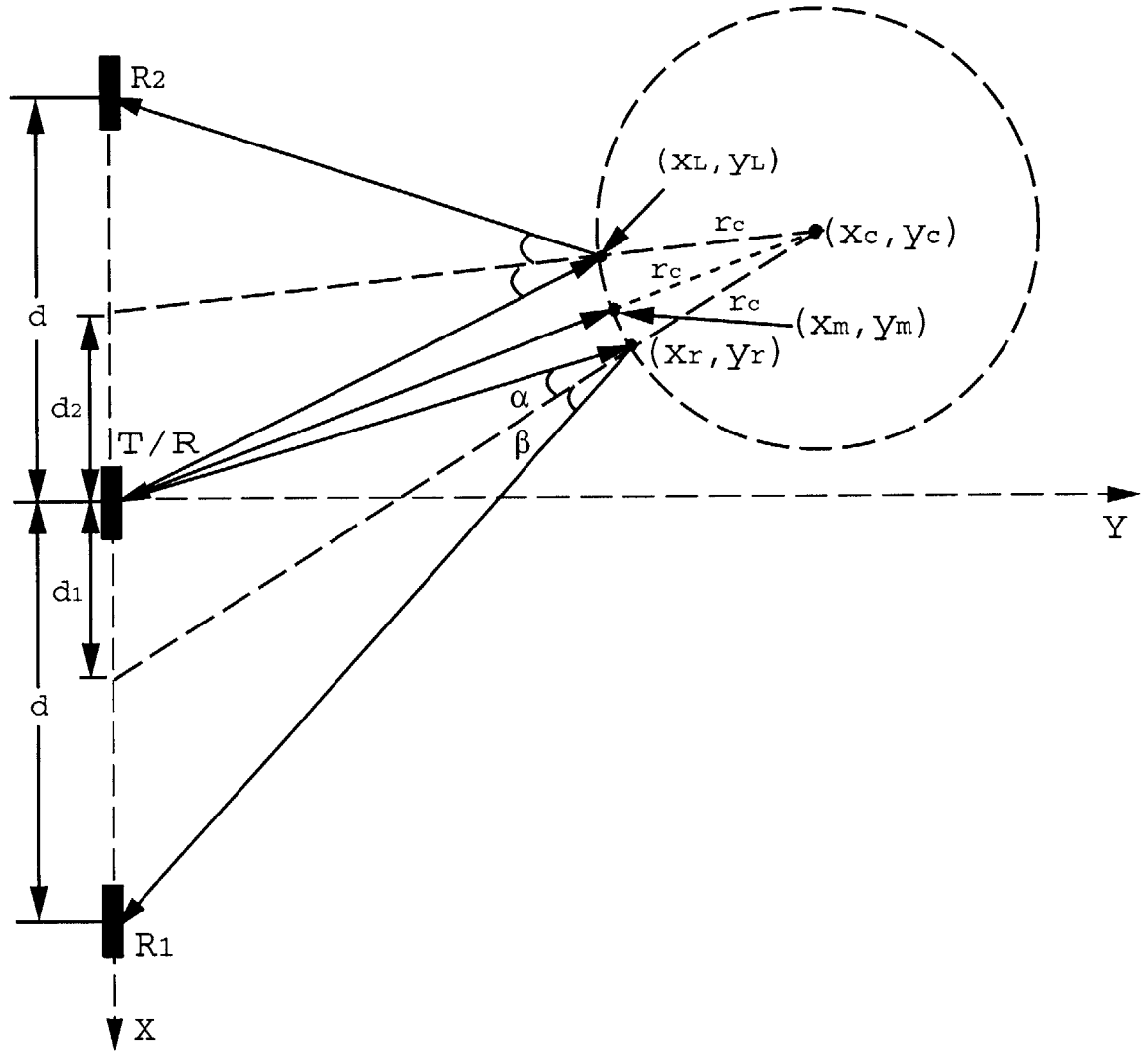

Figure 4-20: Sound travel path from cylinder reflector. This figure defines the parameters used by Equations 4.45 to 4.55.

we have:

$$d_2 \cdot \sqrt{(x_l + d)^2 + y_l^2} = (d - d_2) \cdot \sqrt{x_l^2 + y_l^2} \ , \tag{4.49}$$

$$(x_c + d_2) \cdot y_l = (x_l + d_2) \cdot y_c \ , \tag{4.50}$$

$$(x_c - x_l)^2 + (y_c - y_l)^2 = r_c^2 \ , \tag{4.51}$$

and

$$\sqrt{x_l^2 - y_l^2} + \sqrt{(x_l + d)^2 + y_l^2} = M_l \ . \tag{4.52}$$

For the transmission from center transmitter to center receiver, we have:

$$2\sqrt{x_m^2 - y_m^2} = M_c \ , \tag{4.53}$$

$$(x_c - x_m)^2 + (y_c - y_m)^2 = r_c^2 \ , \tag{4.54}$$

and

$$\frac{x_c}{y_c} = \frac{x_m}{y_m} \ . \tag{4.55}$$

Equations (4.45) to (4.55) represent a group of eleven simultaneous equations with eleven unknowns. These cannot easily be solved analytically. For our results, we have solved them using the function `fsolve()` in the matlab optimization toolbox.

4.3.2 Simulation analysis

The goal of our simulation is to evaluate and compare the two curvature estimation methods. The geometric relationship between the sonar system and the object is similar to Figure 4-5 except that the object is different. This is shown in Figure 4-21. The separation between transducers is set to be 4 cm.

The simulation is studied by three cases:

Case 1: The range and angle of the object are randomly selected. The radius of the object is varied from 0.3 m to 1.5 m in 0.1 m increments. 10 trials are performed

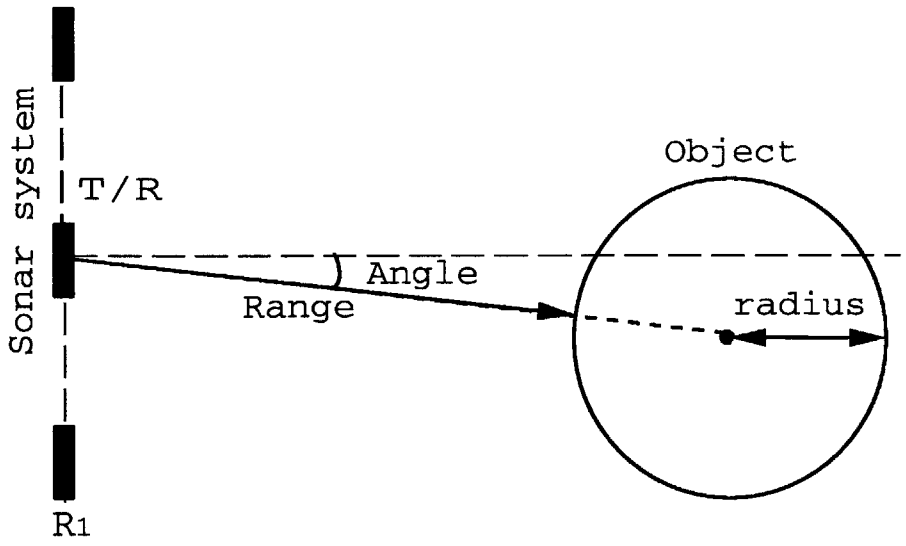

Figure 4-21: Geometry of echolocation for a curvature object

for each radius value. The measurement noise of the three sound travel paths is assumed Gaussian with a standard deviation of 0.002 mm. The estimation results for the two methods is shown in Figure 4-22.

Case 2: The radius and angle of the object are randomly selected. The range of the object is varied from 1.5 m to 3 m in 0.1 m increments. 10 trials are performed for each range value. The measurement noise of the three sound travel paths is assumed Gaussian with a standard deviation 0.002 mm. The estimations result for the two methods is shown in Figure 4-23.

Case 3: The radius and range of the object are randomly selected. The angle of object is varied from 1 degree to 12 degrees in 1 degree increments. 10 trials are performed for each angle value. The measurement noise of the three sound travel paths is assumed Gaussian with a standard deviation of 0.002 mm. The estimation results for the two methods is shown in Figure 4-24.

From Figures 4-22, 4-23, and 4-24, we can see that the radius estimation results obtained by the numerical method are considerably better than those obtained with the approximate method. The angle and range estimation performance of the two methods is similar.

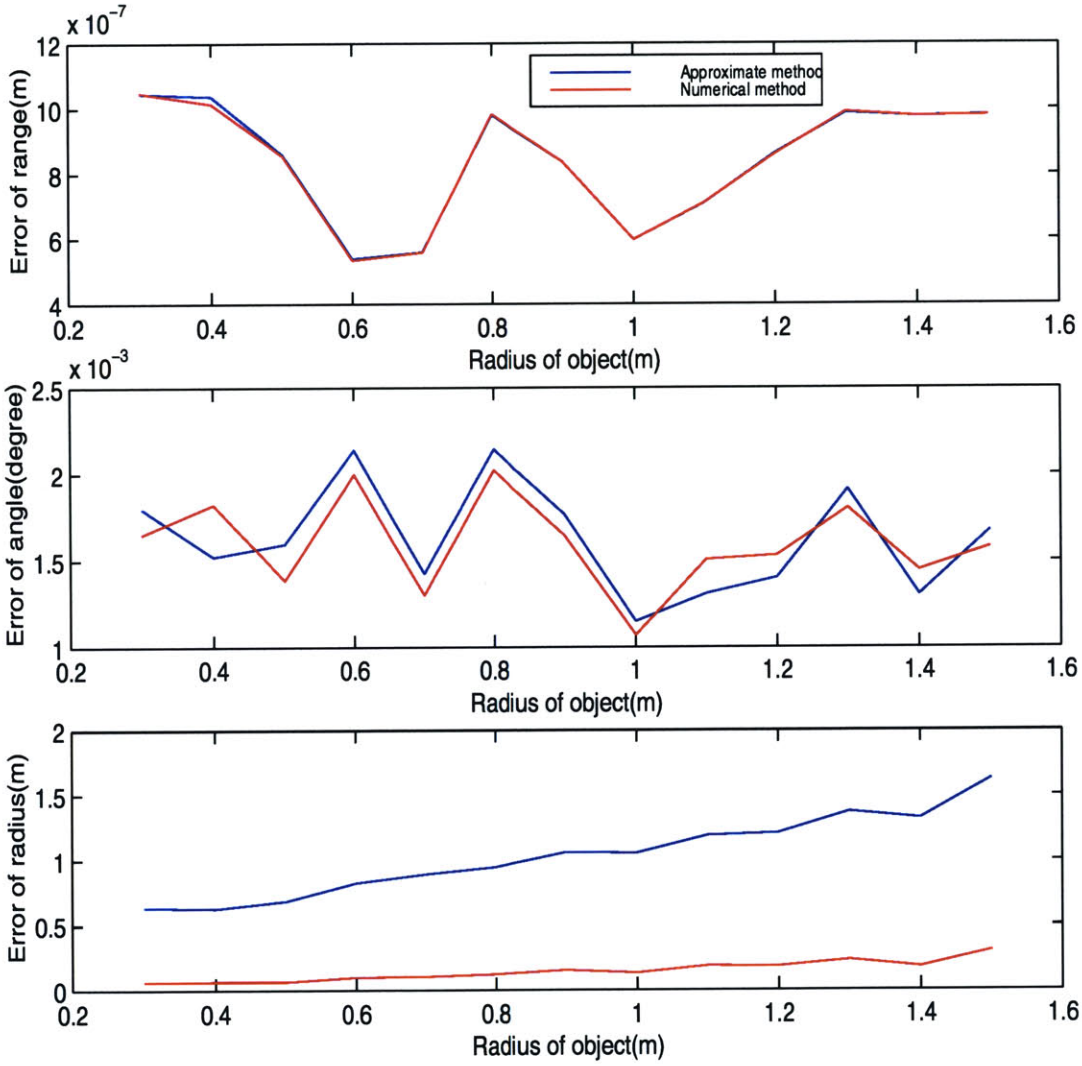

Figure 4-22: A comparison of estimation error vs radius variation by the two localization methods. The range of the object is 3.05 m, the angle of the object is 20.1 degrees.

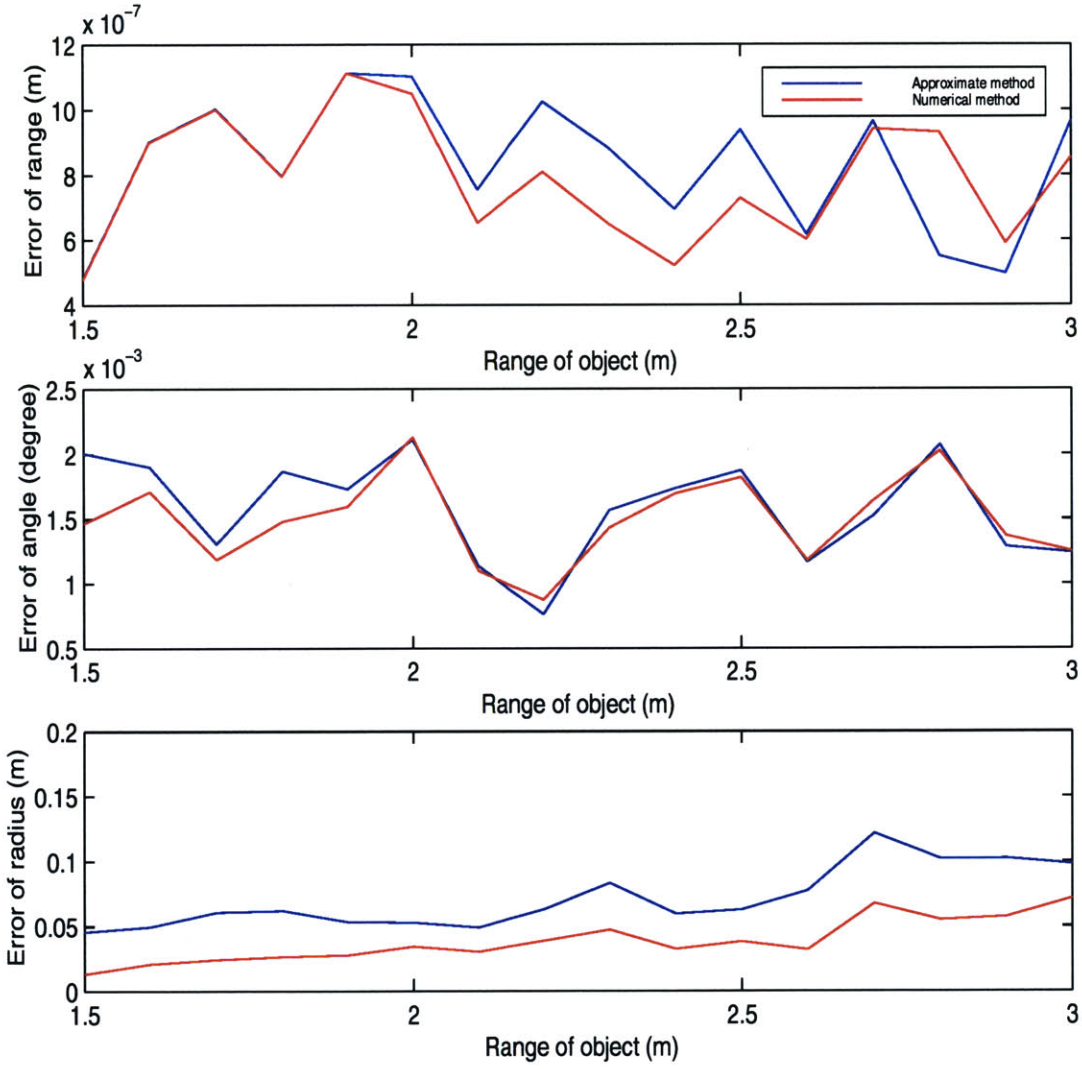

Figure 4-23: A comparison of estimation error vs range variation by the two localization methods. The radius of the object is 0.303 m, the angle of the object is 7.23 degrees.

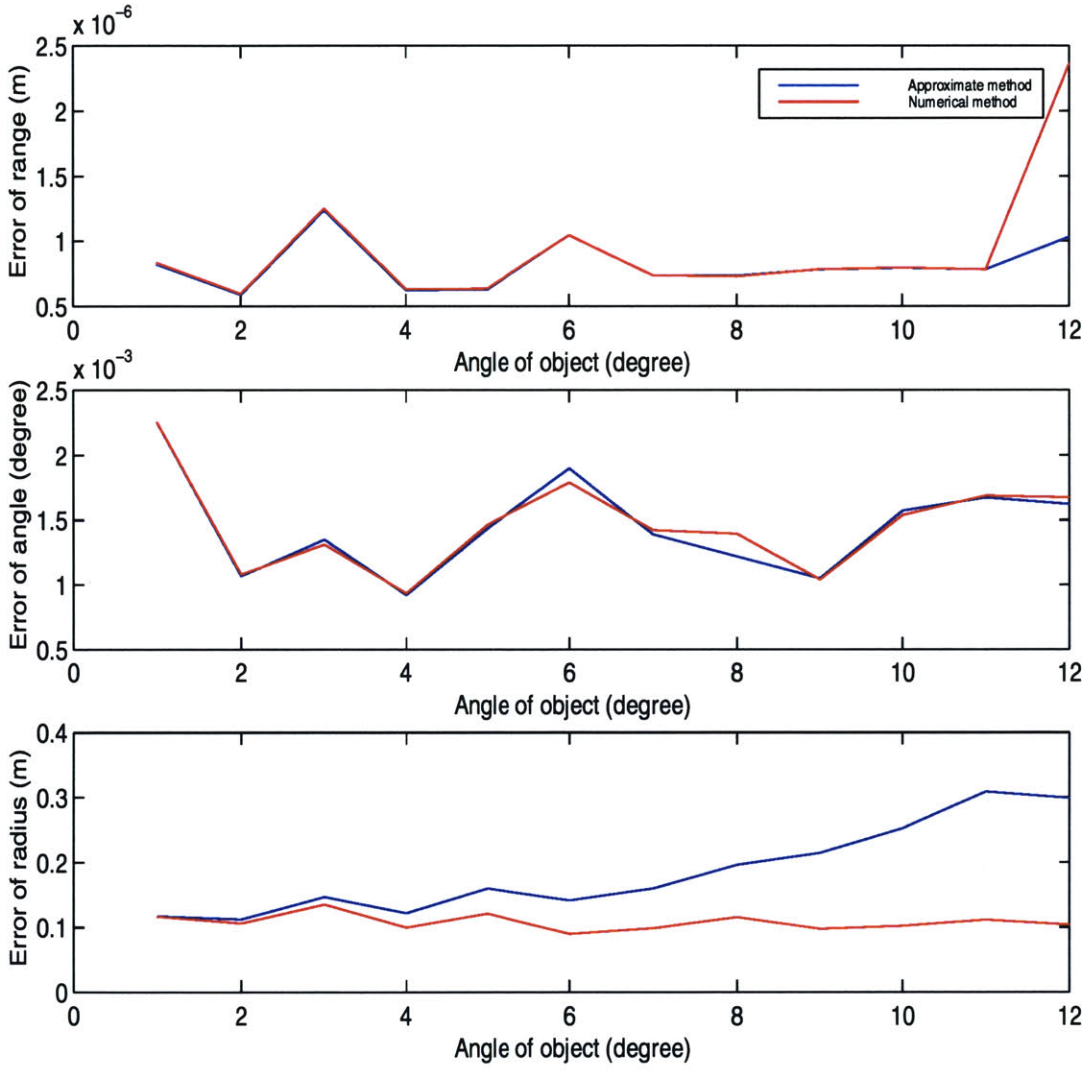

Figure 4-24: A comparison of estimation error vs angle variation by the two localization methods. The radius of the object is 0.66 m, the range of the object is 3.91 m.

4.4 Summary

This chapter has summarized the performance of the system. We compared the performance of matched filter and threshold detectors. We have assessed the accuracy of point object localization. Finally the problem of estimating object curvature was investigated. We have demonstrated with simulation results that a numerical approach performed better than an approximate solution for estimation of the range, angle, and curvature of cylindrical objects. However, sensitivity to noise is still an issue. Our hope is that future research can achieve better curvature information by combining the data obtained by the sensor from different sensing locations.

Chapter 5

Conclusions

This thesis has investigated the use of an underwater biomimetic sonar system for object localization and classification. This chapter concludes the thesis by summarizing the contributions of the thesis research and by making suggestions for future research.

5.1 Contributions

The contributions of the thesis have been the following:

- A wide-beam, wide-band biomimetic binaural sonar has been implemented and tested.
- A variety of signal detection methods have been evaluated.
- The accuracy of object localization using the system has been assessed.
- The problem of estimating object curvature using the system has been investigated.

5.2 Future research

We have many suggestions for improving the system and ideas to investigate in future research. These can be divided into three categories: (1) improved signal detection,

and (2) shape estimation for more complex objects, and (3) adaptive echolocation.

5.2.1 Improved signal detection

Improved signal detection can be achieved by employing more powerful detection techniques and by obtaining a better understanding of the noise of the system. Matched filters provide improved performance but require a detailed knowledge of the received signals. However, for more complex objects, the received echoes can become very complex. The matched filter performance will degrade when the template waveform used does not match the actual object echoes. A simple threshold/energy detector does not make explicit assumptions about the received echo structure, but as we have seen in the previous chapter gives less accurate performance. It has been hypothesized by biosonar researchers that the dolphin sonar system operates like an energy detector [1], but it remains a mystery how the dolphin attains such good performance.

Two alternative ideas to try for improved signal detection are wavelets [38] and neural networks [18]. Wavelets have recently become a popular tool for signal detection in many different application domains. For example, Rodenas and Garello have used wavelets for oceanic synthetic aperture radar data [36]. The performance of a detector strongly depends on the how to represent the signal. If *a priori* information concerning the relative bandwidth and the time-bandwidth-product of the signal is known, a wavelet representation has been proven efficient [17]. Zhang has compared the performance of a discretized wavelet transform (DWT) detector, matched filter detector, and an energy detector [42] for detection of transient ocean events. The DWT detector achieves performance that is almost as good as a matched filter, without requiring knowledge of the structure of the waveform.

There has been a strong interest in the investigation of neural network models for dolphin echolocation. For example, Au and colleagues [2, 3] trained neural networks to perform object recognition and compared the performance with actual dolphin experiments. For our system, it is possible that a neural network detector could be trained to recognize the echoes from different classes of objects, to yield improved localization and classification.

5.2.2 Shape estimation for more complex objects

To estimate the shape of complex objects, it will be necessary to integrate the data obtained from different vantage points. Peremans *et al.* showed that it is difficult to estimate object curvature accurately from a single location using a tri-aural sensor. Hence, motion will be necessary, to collect sonar data from different positions. Moran has investigated curved object shape reconstruction using a single scanning sonar sensor, moved among multiple accurately known positions [30]. The binaural sonar provides more information that can improve the speed and accuracy of such a process. However, uncertain sensor motion add mores many difficulties. Concurrent mapping and localization will be necessary. This has been the subject of Feder's thesis [16]. Future work will use the biomimetic sonar for concurrent mapping and localization with more complex objects.

Reconstruction of objects in three dimensions will require that more degrees of freedom be added to the robotic positioning system in our testing tank. Work is in progress in our facility to add this capability.

5.2.3 Adaptive echolocation

Adaptive combining of sensing and motion can improve the system in two ways, by getting better information and by increased the speed of operation. Sometimes, from one position, the data is ambiguous and difficult to interpret. In adaptive echolocation, the system adaptively move itself according to the echo signals it receives to get better information. In addition, our previous experiments with a single scanning sonar have been very slow, because of the time necessary to take many returns at small angle increments. By using the range, angle, and possibly curvature information, the system can operate more quickly. The same results can be obtained with much less data. It should be possible to track moving objects in real-time. Perhaps one day, the system might even be used to track and catch a fish (just like a real dolphin).

Bibliography

[1] W. Au. *The Sonar of Dolphins.* New York: Springer-Verlag, 1993.

[2] W. W. L Au. Comparison of sonar discrimination: Dolphin and an artificial neural network. *Journal of the Acoustical Society of America*, 95(1):2728–2735, 1994.

[3] W. W. L. Au, L. N. Andersen, A. R. Rasmussen, and P. E. Nachtigall. Neural network modeling of a dolphin's sonar discrimination capabilities. *Journal of the Acoustical Society of America*, 98(1):43–50, July 1995.

[4] W. W. L. Au and P. E. Nachtigall. Dolphin acoustics and echolocation. *Acoustics Bulletin*, 19(4):19–26, July-Aug. 1994. UK.

[5] K. Audenaert, H. Peremans, Y. Kawahara, and J. Van Campenhout. Accurate ranging of multiple objects using ultrasonic sensors. In *Proc. IEEE Int. Conf. Robotics and Automation*, pages 1733–1738, Nice, France, May 1992.

[6] B. Barshan and R. Kuc. Differentiating sonar reflections from corners and planes by employing an intelligent sensor. *IEEE Transactions on Pattern Analysis and Machine Intelligence*, PAMI-12(6):560–569, June 1990.

[7] Billur Barshan. *A sonar-based mobile robot for bat-like prey capture.* PhD thesis, Yale University, 1991.

[8] J. Borenstein and Y. Koren. Obstacle avoidance with ultrasonic sensors. *IEEE Journal of Robotics and Automation*, RA-4:213–218, April 1988.

[9] J. Borenstein and Y. Koren. The vector field histogram – fast obstacle avoidance for mobile robots. *IEEE Journal of Robotics and Automation*, 7(3):278–288, June 1991.

[10] O. Bozma and R. Kuc. Building a sonar map in a specular environment using a single mobile transducer. *IEEE Trans. Pattern Analysis and Machine Intelligence*, 13(12), December 1991.

[11] O. Bozma and R. Kuc. Characterizing pulses reflected from rough surfaces using ultrasound. *J. Acoustical Society of America*, 89(6):2519–2531, June 1991.

[12] O. Bozma and R. Kuc. Characterizing the environment using echo energy, duration, and range: the ENDURA method. In *Proc. IEEE Int. Workshop on Intelligent Robots and Systems*, pages 813–820, 1992.

[13] G. Busnel, editor. *Animal Sonar Systems: Biology and Bionics.* Jouy-en-Josas, France: Laboratoire de Physiologie Acoustique INRA-CNRZ, 1966.

[14] Gage Applied Sciences Corporation. Manual of compuscope 1012/pci a/d board, 1999.

[15] J. F. Engelberger. *Robotics in Service.* Kogan Page, 1989.

[16] H. J. S. Feder. *Simultaneous Stochastic Mapping and Localization.* PhD thesis, Massachusetts Institute of Technology, 1999.

[17] M. Frisch and H. Messer. The use of the wavelet transform in the detection of an unknown transient signal. *IEEE trans. On Information Theory*, 38(2):892–897, March 1992.

[18] S. Haykin. *Neural Networks.* Prentice-Hall, 1993.

[19] K. Higuchi, k. Suzuki, and H. Tanigawa. Ultrasonic phased array transducer for acoustic imaging in air. In *Proceedings IEEE Ultrasonic Symp.*, 1986.

[20] D. Johnson and D. Dudgeon. *Array Signal Processing.* Prentice Hall, 1993.

[21] W. N. Kellogg. *Porpoises and Sonar.* Pheonix Science Series, University of Chicago Press, 1962.

[22] L. Kleeman and R. Kuc. Mobile robot sonar for target localization and classification. *Int. J. Robotics Research*, 14(4), 1995.

[23] R. Kuc. Fusing binaural sonar information for object recognition. In *IEEE/SICE/RSJ International Conference on Multisensor Fusion and Integration for Intelligent Systems*, pages 727–735, 1996.

[24] R. Kuc and M. W. Siegel. Physically based simulation model for acoustic sensor robot navigation. *IEEE Transactions on Pattern Analysis and Machine Intelligence*, PAMI-9(6):766–778, November 1987.

[25] Shin-ichi Kuroda, Akio Jitsumori, and Takahiko Inari. Ultrasonic imaging system for robot using electronic scanning method,. In *Int. Conf. on advanced robotics*, pages 187–193, Japan, 1983.

[26] J. J. Leonard and H. F. Durrant-Whyte. *Directed Sonar Sensing for Mobile Robot Navigation.* Boston: Kluwer Academic Publishers, 1992.

[27] A. Macovski. Ultrasonic imaging using arrays. In H. Lee and G. Wade, editors, *Modern Acoustical Imaging*, pages 217–228. IEEE Press, 1986. Reprinted from *Proc. IEEE*, Volume 67, pp. 484-495, Apr. 1979.

[28] P. Moore and L. Bivens. The bottlenose dolphin: Nature's ATD in SWMCM autonomous sonar platform technology. In *Proceedings of the Autonomous Vehicles in Mine Countermeasures Symposium*, pages 6–63 – 6–67. Naval Postgraduate School, 1995.

[29] P. W. B. Moore, H. L. Roitblat, and P. E. Nachtigall. Recognizing successive dolphin echoes with an integrator gateway network. In *Conference Record of The Twenty-Seventh Asilomar Conference on Signals, Systems and Computers (Cat. No.93CH3312-6).*, volume 1 of *IEEE Comput. Soc. Press. Part*, pages 588–592, Los Alamitos, CA, USA, 1993.

[30] B. A. Moran, J. J. Leonard, and C. Chryssostomidis. Geometric shape from sonar ranging. In *Proc. Int. Symp. on Unmanned Untethered Submersible Technology*, pages 370–383, 1993.

[31] H. Moravec. Sensor fusion in certainty grids for mobile robots. In *Sensor Devices and Systems for Robotics*, pages 253–276. Springer-Verlag, 1989. Nato ASI Series.

[32] W. S. Munro, S. Pomeroy, M. Afiq, M.D . Wybrow, and Wykes. Ultrasonic vehicle guidance transducer. *Ultrasonics*, 28:351–354, 1990.

[33] P. E. Nachtigall, W. W. L. Au, J. L. Pawloski, and H. L. Roitblat. Animal echolocation and signal processing. In *OCEANS 94. Oceans Engineering for Today's Technology and Tomorrow's Preservation. Proceedings (Cat. No.94CH3472-8)*, volume 1 of *IEEE. Part*, pages I/259–263, New York, NY, USA, 1994.

[34] H. Peremans, K. Audenaert, and Campenhout J. M. Van. A high-resolution sensor based on tri-aural perception. *IEEE Transactions on Robotics And Automation*, 9(1):36–48, Feb. 1993. USA.

[35] Arthur N. Popper. *Sound Emission and detection by delphinids.* Robert E. Krieger Publishing Company, 1988.

[36] J. A. Rodenas and R. Garello. Wavelet analysis in sar ocean image profiles for internal wave detection and wavelength estimation. *IEEE Transactions on Geoscience And Remote sensing*, 35(4):933–945, July 1997.

[37] C. M. Smith, J. J. Leonard, A. A. Bennett, and C. Shaw. Concurrent mapping and localization for autonomous underwater vehicles. In *Undersea Defence Technology*, pages 338–342, 1997.

[38] G. S. Strang. *Wavelets and filter banks.* Wellesley, MA: Wellesley-Cambridge Press, 1996.

[39] R. Urick. *Principles of Underwater Sound.* New York: McGraw-Hill, 1983.

[40] P. M. Woodward. *Probability and information theory, with applications to radar.* Oxford: Pergamon Press, 1964. 2nd Edition.

[41] Ming Yang, S. L. Hill, and J. O. Gray. Localization of plane reflectors using a wide-beamwidth ultrasound transducer arrangement. *IEEE Transactions on Instrumentation And Measurement*, 46(3):711–716, June 1997. IEEE.

[42] Y. Zhang. Transient signal detection with an automous underwater vehicle. M.I.T., Feb. 1998. Ph.D thesis proposal.